



This is a repository copy of *Influence of slot/pole number combinations and pole shaping on electromagnetic performance of permanent magnet machines with unbalanced north and south poles.*

White Rose Research Online URL for this paper:

<https://eprints.whiterose.ac.uk/195404/>

Version: Published Version

Article:

Qi, J., Zhu, Z. orcid.org/0000-0001-7175-3307, Jewell, G.W. orcid.org/0000-0002-8763-4190 et al. (5 more authors) (2023) Influence of slot/pole number combinations and pole shaping on electromagnetic performance of permanent magnet machines with unbalanced north and south poles. IET Electric Power Applications. ISSN 1751-8660

<https://doi.org/10.1049/elp2.12293>

Reuse

This article is distributed under the terms of the Creative Commons Attribution-NonCommercial-NoDerivs (CC BY-NC-ND) licence. This licence only allows you to download this work and share it with others as long as you credit the authors, but you can't change the article in any way or use it commercially. More information and the full terms of the licence here: <https://creativecommons.org/licenses/>

Takedown

If you consider content in White Rose Research Online to be in breach of UK law, please notify us by emailing eprints@whiterose.ac.uk including the URL of the record and the reason for the withdrawal request.



eprints@whiterose.ac.uk
<https://eprints.whiterose.ac.uk/>



2nd Advanced Optical Metrology Compendium

Advanced Optical Metrology

Geoscience | Corrosion | Particles | Additive Manufacturing: Metallurgy, Cut Analysis & Porosity



EVIDENT
OLYMPUS

WILEY

The latest eBook from **Advanced Optical Metrology**.
Download for free.

This compendium includes a collection of optical metrology papers, a repository of teaching materials, and instructions on how to publish scientific achievements.



With the aim of improving communication between fundamental research and industrial applications in the field of optical metrology we have collected and organized existing information and made it more accessible and useful for researchers and practitioners.

EVIDENT
OLYMPUS

WILEY

ORIGINAL RESEARCH

Influence of slot/pole number combinations and pole shaping on electromagnetic performance of permanent magnet machines with unbalanced north and south poles

Ji Qi¹ | Ziqiang Zhu¹  | Geraint Wyn Jewell¹  | Luocheng Yan¹ |
Chengwei Gan² | Yuan Ren² | Simon Brockway² | Chris Hilton²

¹Electrical Machines and Drives Group, The University of Sheffield, Sheffield, UK

²Protean Electric Ltd., Farnham, UK

Correspondence

Ziqiang Zhu, Electrical Machines and Drives Group, The University of Sheffield, Mappin Street, Sheffield S1 3JD, UK.

Email: z.q.zhu@sheffield.ac.uk

Funding information

UK EPSRC Future Electrical Machines Manufacturing Hub, Grant/Award Number: EP/S018034/1; Protean Electric Ltd., Grant/Award Number: X/154584-11-1

Abstract

The influences of slot/pole number combinations on electromagnetic performances, including flux linkage, inductance, and torque ripple harmonic components etc., resulting from unbalanced characteristics between north and south poles in concentrated winding permanent magnet (PM) machines with symmetrical and asymmetric rotor pole shaping methods are theoretically analysed and experimentally validated in this paper. It shows that for the PM machines with odd number of coils per phase per submachine, including consequent pole (CP) and surface-mounted PM (SPM) machines, the influences of unbalanced pole characteristics can lead to additional torque ripple harmonics due to additive effects in windings, but can be cancelled in other machines. Compared with symmetrical pole shaping method, asymmetric pole shaping method can result in lower torque ripple for CPPM machines with odd number of coils per phase per submachine, while symmetrical and asymmetric pole shapes have similar effects on torque ripple reduction for other CPPM machines and all the SPM machines. The findings have been validated by finite element analyses on 12-slot/8-pole, 12-slot/10-pole, 9-slot/6-pole, and 12-slot/14-pole machines, and by experiments with 12-slot/8-pole and 12-slot/10-pole CPPM prototypes.

KEYWORDS

consequent pole, fractional slot concentrated winding, permanent magnet machines, pole shaping, torque ripple

1 | INTRODUCTION

Rare-earth permanent magnet (PM) material faces continual challenges of high cost, price fluctuation, and volatile supply, which remain major concerns for rare-earth PM machines [1]. Consequent-pole (CP) PM machines provides a scope to decrease the volume of rare-earth materials in a machine of a given rating and have attracted considerable interest [2–21]. For a consequent pole permanent magnet (CPPM) rotor, alternating poles are formed of iron, while the PMs are in the other poles [2–4]. It was reported in 1978 that CPPM motors can save half of the PM material with only 20% decrease in average torque [4]. In 1986, the consequent pole rotor was pointed out to have the capability to reduce the susceptibility

of the magnet to thermal degradation caused by the heat shrinking operation [5]. There are also dividends in manufacturing costs which can be reduced due to a lower number of PMs in a CPPM rotor [6]. Compared with a conventional surface-mounted PM (SPM) machine, a fractional slot concentrated winding (FSCW) CPPM machine can reduce the volume of PM by over 30% amount with only a small reduction in average torque [7]. Given these advantages, CPPM machines have been identified as promising candidates in a range of applications including injection pumps [8, 9], rope-less elevators [10], and refrigerant compressors [11].

However, even when they are competitive in terms of torque density and/or magnet volume, CPPM machines also have drawbacks, including the large torque ripple [12, 13],

This is an open access article under the terms of the Creative Commons Attribution-NonCommercial-NoDerivs License, which permits use and distribution in any medium, provided the original work is properly cited, the use is non-commercial and no modifications or adaptations are made.

© 2023 The Authors. *IET Electric Power Applications* published by John Wiley & Sons Ltd on behalf of The Institution of Engineering and Technology.

lower average torque [14], axial shaft flux leakage [15], and relatively larger unbalanced magnetic force [16]. Arguably the foremost of these is the large torque ripple in the CPPM structures [17, 18]. It has been found that additional harmonics in back electromotive force (EMF), inductance, and cogging torque resulting from the unbalanced features between iron and PM poles will contribute to the overall torque ripples [12, 13], which in turn gives rise to significant vibration and noise.

To reduce torque ripples, several pole shaping methods have been proposed for CPPM structures. Investigations reported in refs. [12, 13] and demonstrated that different pole shapes between PMs and iron poles as well as asymmetric pole shaping are effective in suppressing the torque ripple for a 12-slot/8-pole (12s8p) CPPM machine. A non-uniform air-gap profiling method has been proposed in ref. [19] but the structure can only be used in outer rotor machines with high pole numbers. In ref. [20], a two-level optimisation method was applied to a six-phase machine to improve torque performance, albeit that the torque ripple of the optimised machine is still larger than that of its SPM counterpart. An alternative approach that optimised the pole-end barrier shape to reduce torque ripple for specific motors was reported in refs. [11, 21]. In ref. [22], an inverse cosine shape air-gap was applied to a CPPM rotor to achieve lower total harmonic distortion (THD) in the air-gap flux density. However, this study was not extended to the comparison of torque performance.

At a more general level, it has been noticed that the torque ripple and back EMF of CPPM machines are comparable to an SPM counterpart when $N_s/m/\text{GCD}(N_s, p)$ is even, where N_s and m are the slot number and the phase number, respectively, and $\text{GCD}(N_s, p)$ is the greatest common divisor (GCD) of slot number and rotor pole-pairs number p [18, 23]. This includes the machine with 48s44p [7], and 24s20p [19]. However, the basic principle of this phenomenon for CPPM machines is still not revealed and analysed in depth. Furthermore, the flux linkage and inductance will also be affected, of which the basic principles have hitherto not been fully investigated. It is unsurprising that such influences will lead to differences in torque ripple components, which will inevitably result in dissimilar torque ripple reduction capabilities of symmetrical and asymmetric pole shaping methods.

In this paper, for general CPPM machines, the effects of slot/pole number combinations on flux linkage, back EMF, and inductance are investigated theoretically, based on which different characteristics of symmetrical and asymmetric pole shaping methods are revealed and validated by the finite element method (FEM) with FSCW 12s8p, 9s6p, 12s10p, and 12s14p CPPM machines as examples. Experiments with 12s8p and 12s10p CPPM prototypes further confirm the analyses.

Such analysis can also be applied to SPM machines with unequal north and south pole widths. Actually, unequal pole widths are commonly utilised to suppress the cogging torque for SPM machines [24, 25] but the performances and pole shaping effects with different slot/pole number combinations have not been investigated. Consequently, the SPM machines will also be analysed in this paper. It will be revealed that

similar to CPPM machines, the harmonics in winding flux linkage will be affected by slot/pole number combinations. However, different from CPPM machines, both symmetrical and asymmetric pole shaping methods have a similar effect on torque ripple reduction for SPM machines due to the absence of reluctance torque ripple.

The contributions and new findings of this paper can be summarised from two aspects:

- 1) When $N_s/m/\text{GCD}(N_s, p)$ is an odd number, the unbalanced pole behaviours will result in additional harmonics in various performances, including flux linkage, back EMF, inductance, cogging torque, and torque ripples for CPPM machine as well as flux linkage, back EMF, cogging torque, and torque ripple for SPM machine. However, such influences can be eliminated in other machines with an even number of $N_s/m/\text{GCD}(N_s, p)$.
- 2) Asymmetric pole shaping method shows a better capability in torque ripple reduction for CPPM machines with $N_s/m/\text{GCD}(N_s, p)$ being an odd number. However, for other machines with an even number of $N_s/m/\text{GCD}(N_s, p)$, including CPPM and SPM machines, the symmetrical pole shaping method has advantages in reducing both torque ripple and optimisation complexity simultaneously.

This paper is organised as follows. Firstly, the influences of slot/pole number combinations on electromagnetic performances of CPPM machines are investigated theoretically in Section 2. Symmetrical and asymmetric pole shaping models and finite element optimisation method for torque ripple reduction are described in Section 3, and applied to the 12s8p, 9s6p, 12s10p, and 12s14p CPPM and SPM machines in Sections 4 and 5 respectively. The performances of CPPM and SPM machines are compared in Section 6. This is followed by experimental verification in Section 7 and the conclusions in Section 8.

2 | TOPOLOGIES AND EFFECT OF SLOT/POLE NUMBER COMBINATIONS ON ELECTROMAGNETIC PERFORMANCES

2.1 | Slot/pole number combinations for CPPM machines

An FSCW machine with balanced phase windings can be divided into N_{sp} identical submachines:

$$N_{sp} = \text{GCD}(N_s, p)/\nu \quad (1)$$

where N_s is the slot number, p is the pole-pair number, and ν is 1 or 2 for double layer (DL) or single layer (SL) windings.

The FSCW machines can be separated into two groups according to the coil number for one phase in a submachine, $N_s/\nu/m/N_{sp}$, that is, $N_s/m/\text{GCD}(N_s, p)$, equal to an odd number (2), or an even number (3):

$$\text{Group 1} \quad \frac{N_s}{m\text{GCD}(N_s, p)} = 2k - 1, (k = 1, 2, 3 \dots) \quad (2)$$

$$\text{Group 2} \quad \frac{N_s}{m\text{GCD}(N_s, p)} = 2k, (k = 1, 2, 3 \dots) \quad (3)$$

For 3-phase FSCW machines ($m = 3$), the machines with 12s8p-DL ($N_{sp} = 4$), 9s6p-DL ($N_{sp} = 3$), and 12s8p-SL ($N_{sp} = 2$), Figure 1a, belong to the first group. In this group, the number of coils that are allocated to the same phase in one submachine is an odd number as demonstrated in Figure 2a and Table 1. As will be seen later, for the first group of machines, unbalanced features between north and south poles can produce winding flux linkage harmonics for both SPM and CPPM machines and inductance harmonics for CPPM machines.

On the other hand, the machines with 12s10p-DL ($N_{sp} = 1$), 12s14p-DL ($N_{sp} = 1$), and 12s10p-SL ($N_{sp} = 1$) belong to the second group, Figure 1b, and the number of coils that are allocated to the same phase in one submachine is an even number as demonstrated in Figure 2b and Table 1. As shown in Figure 2b, there exist the coils with a 180-electrical-degree difference and

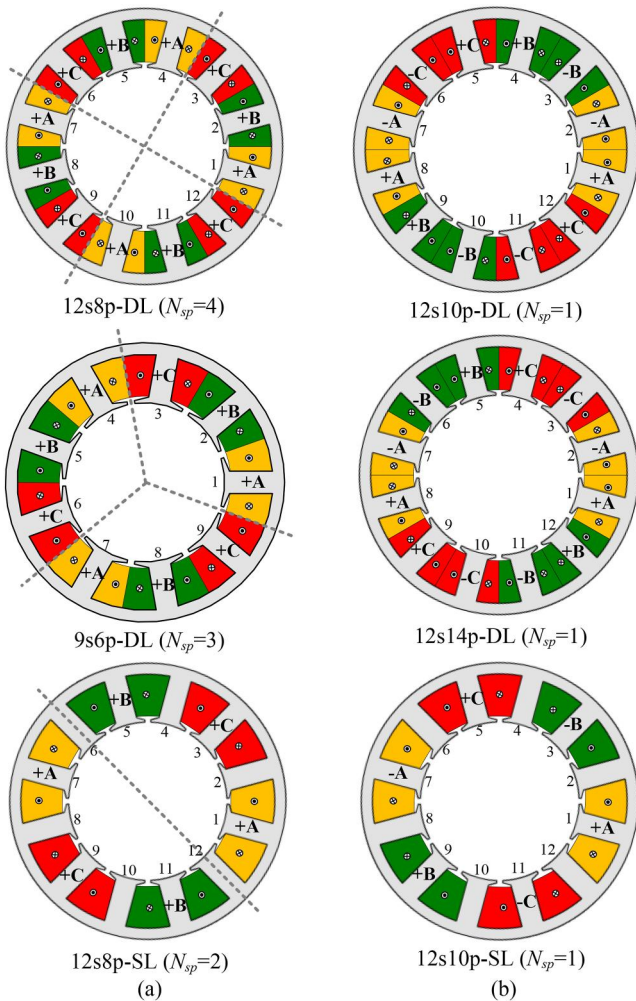


FIGURE 1 Stator winding layouts. (a) Group 1, (b) Group 2.

they are allocated into the same phase to achieve a high winding factor, as is the same case in ref. [26]. Consequently, for the second group of machines, harmonics in winding flux linkage and inductance caused by unbalanced features between north and south poles can be cancelled. This will be analysed in detail in the following parts.

This classification can be applied to both SPM and CPPM machines, and their rotor structures are illustrated in Figure 3. It is worth noting that the unbalanced north and south poles are more common in CPPM machines. Therefore, the following analysis will particularly refer to CPPM machines.

2.2 | Analysis of flux linkage and inductance harmonics and torque ripple for CPPM machines

2.2.1 | Harmonics in flux linkage and inductance

The double layer winding machines are demonstrated as the example in the following analysis, while the phenomenon, principles, and conclusions of double layer machines can be equally applied to the single layer winding machines.

The features of north and south poles in CPPM machines are unequal even if the PM and iron pole widths are the same and it will inevitably result in even order harmonics in air-gap flux density [18] and odd order harmonics in the inductance of a coil [27]. However, additional harmonics do not always exist

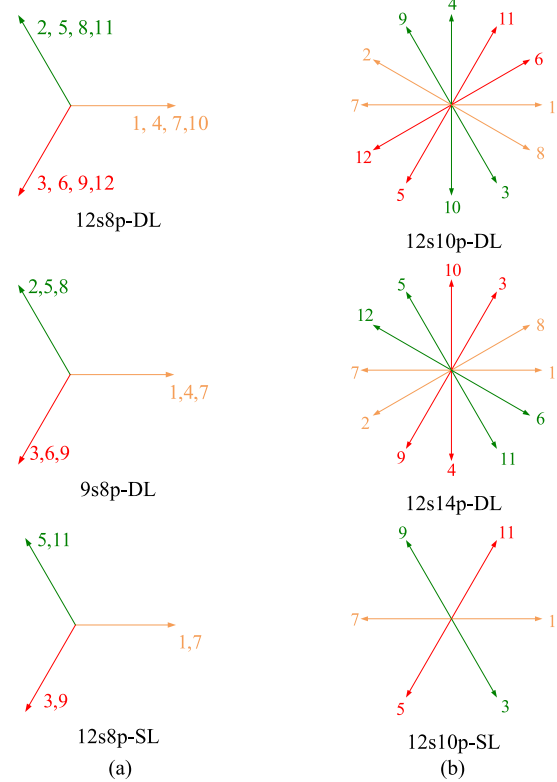
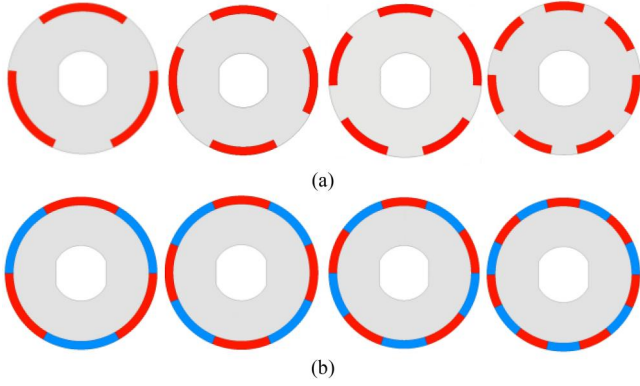


FIGURE 2 Back EMF phasors of coils. (a) Group 1, (b) Group 2. EMF, electromotive force.

TABLE 1 Number of submachine and coils per phase in a submachine for machines in two groups

Slot/pole	Group 1			Group 2		
	12s8p-DL	9s6p-DL	12s8p-SL	12s10p-DL	12s14p-DL	12s10p-SL
N_{sp}	4	3	2	1	1	1
$N_s/m/\text{GCD}(N_s, p)$	1	1	1	4	4	2

**FIGURE 3** Rotor topologies (from left to right: 6p, 8p, 10p, and 14p). (a) CPPM, (b) SPM. CPPM, consequent pole permanent magnet; SPM, surface-mounted permanent magnet.

in winding flux linkage and winding inductance. This is affected by the coil connection that is determined by slot/pole number combinations.

For the first group CPPM machines, the even order harmonics in winding flux linkage and odd order harmonics in winding inductance can be produced due to additive effect of phase coils, while those for the second group CPPM machines can be eliminated due to cancellation effect of phase coils. The derivation process can be explained below.

The phasor angle α_{ij} between the i th and the j th coils can be written as:

$$\alpha_{ij} = (i - j)p \frac{2\pi}{N_s} \quad (4)$$

For the second group CPPM machines, supposing the i th and the j th coils are in the same phase and a submachine, the relation between the numbers of the i th and the j th coils can be expressed by:

$$i - j = \frac{N_s}{2\text{GCD}(N_s, p)} \quad (5)$$

Because the coil number for one phase in a submachine is an even number for both double and single layer winding machines, each i th coil has its corresponding j th coil in the same phase, which has 180-electrical-degree difference to achieve high winding factors, as illustrated in Figure 2b. Consequently, the even order harmonics in flux linkages of i th and j th coils will be eliminated, which can be expressed as:

$$\begin{aligned} \psi_{2n}^i - \psi_{2n}^j &= \psi_{2n} \left[\sin \left(2nip \frac{2\pi}{N_s} + \theta_{2n}^{\psi} \right) \right. \\ &\quad \left. - \sin \left(2nip \frac{2\pi}{N_s} + 2n\pi \frac{p}{\text{GCD}(N_s, p)} + \theta_{2n}^{\psi} \right) \right] = 0 \end{aligned} \quad (6)$$

where ψ_{2n}^i and ψ_{2n}^j are the $2n$ -order harmonics in flux linkages of the i th and the j th coils, respectively, ψ_{2n} and θ_{2n}^{ψ} are the amplitude and the initial position angle of the $2n$ -order harmonic. It is worth noting that the item $p/\text{GCD}(N_s, p)$ in Equation (6) is an odd number when Equation (3) is satisfied.

For the odd order harmonics in flux densities, including the fundamental order harmonic, they will not be affected by the winding connection since:

$$\begin{aligned} \psi_{2n-1}^i - \psi_{2n-1}^j &= \psi_{2n-1} \left[\sin \left((2n-1)ip \frac{2\pi}{N_s} + \theta_{2n-1}^{\psi} \right) \right. \\ &\quad \left. - \sin \left((2n-1)ip \frac{2\pi}{N_s} \right. \right. \\ &\quad \left. \left. + (2n-1)\pi \frac{p}{\text{GCD}(N_s, p)} + \theta_{2n-1}^{\psi} \right) \right] \\ &= 2\psi_{2n-1} \sin \left((2n-1)ip \frac{2\pi}{N_s} + \theta_{2n-1}^{\psi} \right) \end{aligned} \quad (7)$$

The inductance harmonics can also be derived similarly. It has been found that the inductance in one coil consists of all orders of harmonics in CPPM machines due to only one salient pole in an electrical cycle for a CPPM rotor [27]. However, when the coil number for one phase in a submachine is an even number, namely the second group CPPM machines, the odd order harmonics in inductances of the i th and j th coils will be eliminated since

$$\begin{aligned} L_{2n-1}^i + L_{2n-1}^j &= L_{2n-1} \left[\sin \left((2n-1)ip \frac{2\pi}{N_s} + \theta_{2n-1}^L \right) \right. \\ &\quad \left. + \sin \left((2n-1)ip \frac{2\pi}{N_s} \right. \right. \\ &\quad \left. \left. + (2n-1)\pi \frac{p}{\text{GCD}(N_s, p)} + \theta_{2n-1}^L \right) \right] = 0 \end{aligned} \quad (8)$$

where L_{2n-1}^i, L_{2n-1}^j are the $2n$ -order harmonics in inductances of the i th and the j th coils, respectively, L_{2n-1} and θ_{2n-1}^L are the amplitude and the initial position angle of $2n$ -order harmonic.

Since each i th coil has its corresponding j th coil, the odd order harmonics in inductance can be eliminated. However, the even order harmonics still exist:

$$\begin{aligned} L_{2n}^i + L_{2n}^j &= L_{2n} \left[\sin\left(2nip\frac{2\pi}{N_s} + \theta_{2n}^L\right) \right. \\ &\quad \left. + \sin\left(2nip\frac{2\pi}{N_s} + 2n\pi\frac{p}{\text{GCD}(N_s, p)} + \theta_{2n}^L\right) \right] \\ &= 2L_{2n} \sin\left(2nip\frac{2\pi}{N_s} + \theta_{2n}^L\right) \end{aligned} \quad (9)$$

From the above analyses, it can be concluded that for the second group CPPM machines, the even order harmonics in flux linkage and odd order harmonics in winding inductance can be eliminated, which makes it similar to the SPM counterparts.

However, for the first group CP, whose slot/pole numbers can be expressed by Equation (2), there will be no coupling between the i th and j th coils which have the opposite phasors allocated in the same phase, as can be seen in Figure 2a. Therefore, Equations (6) and (8) cannot be 0 anymore, which will lead to the additional even order harmonics in flux linkage and the odd order harmonics in inductance. The different electromagnetic characteristics found in specific CPPM machines in Refs. [7, 12, 18, 19, 27] underpin the above theoretic analysis and the general conclusions.

2.2.2 | Torque ripple production

The even order harmonics in flux linkage and the odd order harmonics in inductance of CPPM machines will inevitably lead to torque ripples. To make it clear, the output torque T_e can be divided into three constituent components: PM torque T_{PM} , reluctance torque T_r , and cogging torque T_{cog} . These can be expressed as [28, 29]:

$$\begin{cases} T_e = T_{PM} + T_r + T_{cog} \\ T_{PM} = \frac{3}{2}pi_q \left(\psi_d^{PM} + \frac{d\psi_q^{PM}}{d\theta} \right) - \frac{3}{2}pi_d \left(\psi_q^{PM} - \frac{d\psi_d^{PM}}{d\theta} \right) \\ T_r = \frac{3}{2}p \left(i_q i_d (L_d - L_q) + i_d^2 \frac{dL_d}{d\theta} + i_q^2 \frac{dL_q}{d\theta} \right) \\ T_{cog} = -\frac{dW_r(\theta)}{d\theta} \end{cases} \quad (10)$$

where L_d and L_q are the dq -axis inductances, i_d and i_q are the dq -axis currents, ψ_d^{PM} and ψ_q^{PM} are the dq -axis PM flux linkages, p is the pole-pair number, θ is the rotor position in electrical degree, and $W_r(\theta)$ is the magnetic co-energy solely due to PM flux linkage. Evidently, the variations in dq -axis PM

flux linkages, dq -axis inductances, and $W_r(\theta)$ will lead to the total torque ripple.

A detailed analysis has been developed in ref. [13] that the odd order harmonics in inductance can contribute to the dominant third and high order ripple in reluctance torque T_r . Therefore, the elimination of odd order harmonics in inductance will result in the cancelation of those additional reluctance torque ripples. Since the production of torque ripple in T_r has been demonstrated in ref. [13], in this paper, with a similar method adopted, only the production of torque ripple in T_{PM} and cogging torque will be derived as follows.

The even order harmonics in flux linkage ψ_{abc} for CPPM machines can be expressed as:

$$\psi_{abc} = \begin{bmatrix} \sum_{n=2,4,6,\dots} \psi_{an} \cos(n\theta) \\ \sum_{n=2,4,6,\dots} \psi_{an} \cos\left(n\left(\theta - \frac{2\pi}{3}\right)\right) \\ \sum_{n=2,4,6,\dots} \psi_{an} \cos\left(n\left(\theta + \frac{2\pi}{3}\right)\right) \end{bmatrix} \quad (11)$$

where ψ_{an} is the amplitude of the n -order harmonic. Then, the d - and q -axis flux linkages ψ_{dq} can be derived as:

$$\psi_{dq} = P\psi_{abc} \quad (12)$$

where

$$P = \frac{2}{3} \begin{bmatrix} \cos(\theta) & \cos(\theta - 2\pi/3) & \cos(\theta + 2\pi/3) \\ -\sin(\theta) & -\sin(\theta - 2\pi/3) & -\sin(\theta + 2\pi/3) \\ 0.5 & 0.5 & 0.5 \end{bmatrix} \quad (13)$$

Therefore, the harmonics in ψ_d and ψ_q resulted from the even order harmonics in ψ_{abc} can be written as:

$$\begin{cases} \psi_d = \sum_{j=1,3,5,\dots} \psi_{adj} \cos(3j\theta) \\ \psi_q = \sum_{j=1,3,5,\dots} \psi_{aqj} \sin(3j\theta) \end{cases} \quad (14)$$

where ψ_{adj} and ψ_{aqj} are the corresponding amplitudes of $3j$ -order harmonics. Obviously, the even order harmonics will lead to the additional $3j$ th order harmonics in ψ_d and ψ_q , which will inevitably result in the corresponding harmonics in PM torque ripple according to (10). Therefore, the first group CPPM machines will suffer from the triplet order harmonics in T_{PM} . However, for the second group CPPM machines, the elimination of even order harmonics in flux linkages will contribute to the same harmonic orders, that is, the multiple of 6, as SPM machines in T_{PM} .

Due to the effect of even order harmonics in flux density, the cogging torque cycle number in a mechanical rotation cycle

for CPPM machines is the least common multiple (LCM) between slot number N_s and pole-pair number p . Based on the relation between LCM and GCD:

$$\text{LCM}(N_s, p)\text{GCD}(N_s, p) = N_s p \quad (15)$$

Equation (3) can be rewritten as:

$$\text{LCM}(N_s, p) = 2kmp, (k = 1, 2, 3, \dots) \quad (16)$$

It is obvious that $2kmp$ is also multiple of $2p$:

$$\text{LCM}(N_s, 2p) = \text{LCM}(N_s, p) = 2kmp, (k = 1, 2, 3, \dots) \quad (17)$$

Since $\text{LCM}(N_s, 2p)$ is the fundamental order of cogging torque for the conventional SPM machines with equal north and south pole arc widths [30, 31], the fundamental cogging torque cycle number for CPPM machines is the same as that for SPM counterparts. In other words, the influence of even order harmonics in flux density on the cogging torque harmonics can be eliminated for the CPPM machines in the second group. In contrast, for CPPM machines in the first group, the fundamental order for cogging torque is halved and there exist additional harmonics.

2.3 | Analysis of flux linkage and inductance harmonics and torque ripples for SPM machines

Similar to CPPM machines, when north and south pole arc widths are different for SPM machines, the even order harmonics in air-gap flux density can produce corresponding harmonics in winding flux linkages for the first group SPM machines. Therefore, it will lead to additional odd order PM torque ripples according to (10). However, such harmonics can be cancelled in the second group SPM machines as has been explained in Equations (6) and (7). It is worth noting that when the SPM machines have equal north and south pole arc widths, the even order harmonics in air-gap flux density can be eliminated and thus even order harmonics in winding flux linkage are eliminated.

When machine geometries are fixed, the cogging torque is determined by the air-gap flux density [30, 31]. Thus, for SPM machines with unequal north and south pole arc widths, the characteristic of cogging torque harmonics are the same as that for CPPM machines, that is, the first group of SPM machines has lower fundamental harmonic $\text{LCM}(N_s, p)$, while that for the second group SPM machines is $\text{LCM}(N_s, 2p)$. The latter one is the same as conventional SPM machines with equal north and south pole arc widths.

Nevertheless, different from CPPM machines, the inductance for SPM machines can be treated as constant since there is no iron saliency in the rotor. Consequently, SPM machines are inherently free of inductance harmonics, and thus, there are

no ripples in reluctance torque not matter whether the north and south poles have equal or unequal arc widths.

To validate the analysis, CPPM and SPM machines for the first group (12s8p and 9s6p as examples) and the second group (12s10p and 12s14p as examples) machines are analysed by FEM. The SPM machines with both equal and unequal north and south pole arc widths are analysed and the names of the latter ones are suffixed with ‘un’ in Figures 4 and 5. For all SPM machines with unequal pole widths and CPPM machines, the ratios of PM pole arc to pole pitch are set as 1.2. As shown in Figures 4 and 5, the harmonics in flux densities, winding flux linkages, coil inductances, winding inductances, cogging torques, on-load PM torque, on-load reluctance torque, and rated torques are illustrated, where the frozen permeability method in ref. [32] is adopted to obtain the on-load reluctance torques and on-load PM torques.

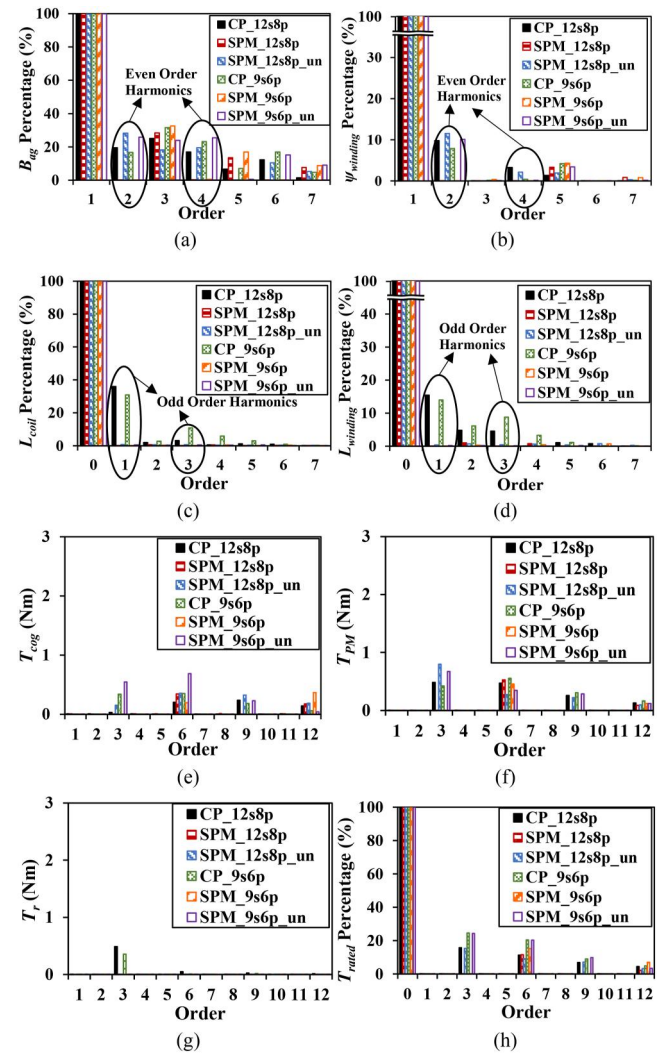


FIGURE 4 Harmonics in one electrical cycle for Group 1 machines. (a) Air-gap flux density B_{ag} , (b) Winding flux linkage $\psi_{winding}$, (c) Coil inductance L_{coils} , (d) Winding inductance $L_{winding}$, (e) No-load cogging torque T_{cog} , (f) On-load PM torque T_{PM} , (g) On-load reluctance torque T_r , and (h) Rated torque T_{rated} .

For the first group of machines, Figure 4, it can be found that the even order harmonics in air-gap flux densities can produce corresponding harmonics in winding flux linkages regardless of whether they are SPM or CPPM machines. Only the SPM machine with equal pole arc widths can eliminate those even order harmonics, Figure 4a,b. Such harmonics can lead to odd order PM torque ripples as illustrated in Figure 4f. However, differently, there are no odd order harmonics in inductances for all SPM machines while such harmonics are obvious for CPPM machines, Figure 4c,d, thus leading to the significant odd order reluctance torque ripple for CPPM machines, Figure 4g. As can be seen in Figure 4h, the overall torque ripple harmonic orders are the multiple of 3 for SPM machines with unequal pole widths and CPPM machines, while they are the multiple of 6 for conventional SPM machines with equal pole widths.

For the second group of machines, Figure 5, it is obvious that the even order harmonics in winding flux linkage and the odd order harmonics in winding inductances can be eliminated for all the CPPM and SPM machines with equal and unequal pole arc widths. Therefore, for all the machines, the PM torque ripple harmonic orders are the multiple of 6 and the reluctance torque ripples are nearly 0. As can be seen in Figure 5h, the overall torque ripple harmonic orders are the multiple of 6. The FEM results prove the analyses very well.

3 | TORQUE RIPPLE REDUCTION WITH SYMMETRICAL AND ASYMMETRIC POLE SHAPING METHODS AND OPTIMISATION RESULT ANALYSIS

3.1 | Symmetrical and asymmetric pole shaping methods

Based on the above analysis, from the perspective of torque ripple, it can be concluded that the first group CPPM machines will be affected by the unbalanced features and suffer from the additional torque ripples, including the third and the ninth. However, the second group CPPM machines have the same torque ripple harmonics as SPM machines, which means the CPPM machines in the second group can overcome the unbalanced features caused by PM and iron poles due to cancelation effect by the arrangement of coils. Therefore, the pole shaping methods for these two types of CPPM machines should be different.

The pole shaping methods largely modify the harmonics of PM flux density, including amplitudes and phases, which have little effect on the fundamental self-inductance since there is only one salient pole in one pole-pair of the CPPM rotor. Consequently, for the first group CPPM machines, introducing the unbalance in flux density (even order harmonics) and manipulating the phases of harmonics to make torque ripple components cancel with each other is an effective means of eliminating the triplet order total torque ripple.

As shown in Figure 6, the symmetrical flux density B_{fs} and the asymmetric flux density B_{fa} can be written as:

$$B_{fs} = \sum_{i=1}^{\infty} A_{si} \cos\left(\frac{p}{2} i \theta\right) \quad (18)$$

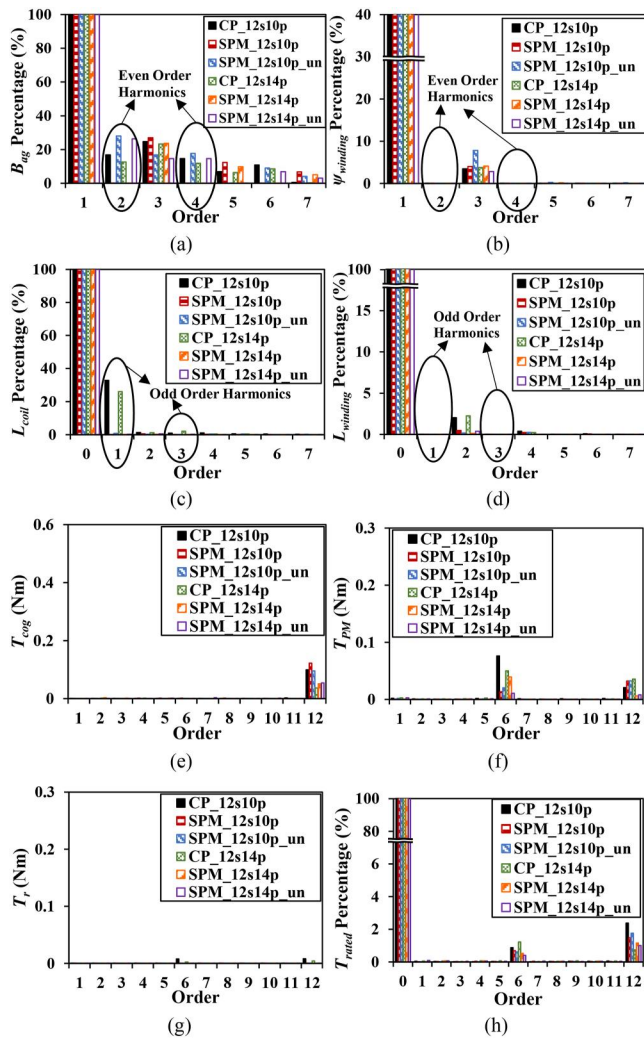


FIGURE 5 Harmonics in one electrical cycle for Group 2 machines. (a) Air-gap flux density B_{ag} , (b) Winding flux linkage $\psi_{windings}$, (c) Coil inductance L_{coil} , (d) Winding inductance $L_{winding}$, (e) No-load cogging torque T_{cog} , (f) On-load PM torque T_{cog} , (g) On-load reluctance torque T_r , and (h) Rated torque T_{rated} .

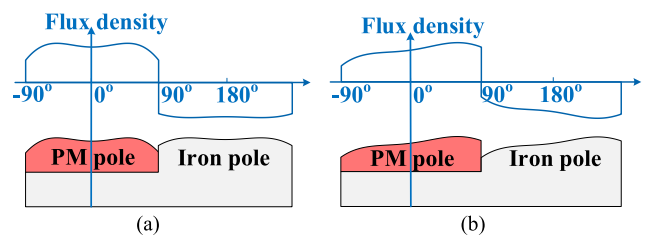


FIGURE 6 Flux density distributions under one pole-pair. (a) Symmetrical, (b) Asymmetric.

$$B_{fa} = \sum_{i=0}^{\infty} A_{aci} \cos\left(\frac{p}{2}i\theta + \theta_{i0}\right) \quad (19)$$

where A_{si} and A_{aci} are the amplitudes of the i th harmonics for symmetrical and asymmetric models, respectively, and θ_{i0} is the phase angle for each harmonic.

Obviously, the phase angle for each harmonic in B_{fs} is fixed, while it is variable in B_{fa} . It can be found that by shifting the phases of flux density harmonics, it is possible to shift the phase of winding flux linkage and thus the torque ripple harmonics in T_{PM} and T_{cog} . Consequently, these torque ripple harmonics can be manipulated to counteract the torque ripple in T_r to reduce the overall torque ripple. Therefore, the asymmetric pole shaping method for CPPM machines in the first group CPPM machines, for example, 12s8p machines [13], can reduce torque ripple effectively.

Nevertheless, the torque ripple characteristics of CPPM machines in the second group, for example, 12s10p, are close to those of their SPM counterparts and can overcome the unbalanced features resulting from the CPPM rotor. Therefore, the PM pole arc can be extended to maximise the output torque without introducing additional torque ripple harmonics. Furthermore, asymmetric pole shape is not necessary since it is just used for overcoming the effects of unbalance in pole behaviours for the CPPM machines in the first group. It is unsurprising that the adoptions of symmetrical and asymmetric pole shapes tend to exhibit similar capacities in torque ripple reduction since the phase shift resulting from asymmetric pole shape has little effect on the PM torque ripple amplitudes and it has almost no reluctance torque component to be counteracted.

The characteristics of torque ripples and their reduction methods for two groups of CPPM machines are summarised in Table 2.

It is worth mentioning that the pole shaping effects on SPM machines are similar to those of the second group CPPM

machines. Since there is no reluctance torque ripple, it is impossible to make PM torque ripple and reluctance torque ripple counteract each other by the asymmetric pole shaping method. Consequently, the adoptions of symmetrical and asymmetric pole shapes tend to exhibit similar capabilities in torque ripple reduction. The characteristics of torque ripples and their reduction methods for two groups of SPM machines are summarised in Table 3.

Figure 7a,b illustrate the modelling method of symmetrical and asymmetric pole shapes in ANSYS Maxwell, respectively. Clearly, both poles (PM and iron poles for CPPM machines, north and south poles for SPM machines) are shaped and the rotor pole profiles are determined by the corresponding pole arc spans as well as the radius of k th point in north pole Rm_k and in south pole Ri_k for CPPM machines, which are distributed uniformly along the circumferential angle. As has been proven effective in Ref. [13], 14 variable points over one pole-pair are adopted in this paper, which are connected by spline curves for each pole. Supposing θm_p and θi_p are the arc span angle of north and south pole as demonstrated in Figure 7, the position for the k th point in the two models is determined by:

$$\begin{cases} \theta m_k = \frac{k-1}{6} \theta m_p, k \in [1, 7] \text{ or } k \in [1, 4] \\ \theta i_k = \frac{k-1}{6} \theta i_p, k \in [1, 7] \text{ or } k \in [1, 4] \\ R_{ri} < Ri_k < R_{ro}, R_{ri} < Rm_k < R_{ro} \end{cases} \quad (20)$$

where R_{ro} and R_{ri} are the outer and inner radii of the rotor, respectively, θm_k and θi_k determine the angle of each point in north and south poles to the left side of each pole. It is worth noting that for symmetrical model, there are only four points, which formed as equivalent seven points over one pole. The reduced variable number can, to some extent, lead to the benefits of time saving in the design process.

TABLE 2 Summaries of torque ripple characteristics and reduction methods for CPPM machines in two groups

Group 1 CPPM machines for example, 12s8p, 9s6p, 9s8p etc.		Group 2 CPPM machines for example, 12s10p, 12s14p, 6s10p etc.
Sources of torque ripple	T_{PM} Even order harmonics in air-gap flux density can produce even order harmonics in winding flux linkage, which will lead to triplen ripples in T_{PM}	Even order harmonics in air-gap flux density cannot produce even order harmonics in winding flux linkage, which makes the ripple orders of T_{PM} a multiple of 6 regardless of whether PM and iron poles are equal or unequal in width
	T_r The odd order harmonics in winding inductance will lead to triplen ripples in T_r	The odd order harmonics in winding inductance can be cancelled and torque ripple orders of T_r are the multiple of 6 which are the same as those of conventional SPM machines with equal north and south pole widths
	T_{cog} The fundamental cycle number is half of that of conventional SPM counterpart with equal pole widths	The fundamental cycle number is the same as that of conventional SPM counterpart with equal pole widths
Torque ripple reduction	Different from symmetrical pole shaping method, asymmetric pole shaping method can make the torque ripple components counteract each other and lead to a smaller overall torque ripple	Asymmetric and symmetrical profiles have a similar capacity in torque ripple reduction

Abbreviations: CPPM, consequent pole permanent magnet, SPM, surface-mounted permanent magnet.

TABLE 3 Summaries of torque ripple characteristics and reduction methods for SPM machines in two groups

Group 1—SPM machines for example, 12s8p, 9s6p, 9s8p etc. etc.		Group 2—SPM machines for example, 12s10p, 12s14p, 6s10p
Sources of torque ripple	T_{PM} Even order harmonics in air-gap flux density can produce even order harmonics in winding flux linkage, which will lead to triplen ripples in T_{PM}	Even order harmonics in air-gap flux density cannot produce even order harmonics in winding flux linkage, which makes the ripple orders of T_{PM} a multiple of 6 regardless of whether north and south poles are equal or unequal in width
	T_r There are no harmonics in winding inductance and thus no reluctance torque ripple	
	T_{cog} The fundamental cycle number is half of that of conventional SPM counterpart with equal pole widths	The fundamental cycle number is the same as that of conventional SPM counterpart with equal pole widths
Torque ripple reduction	Asymmetric and symmetrical profiles have a similar capacity in torque ripple reduction	

Abbreviation: SPM, surface-mounted permanent magnet.

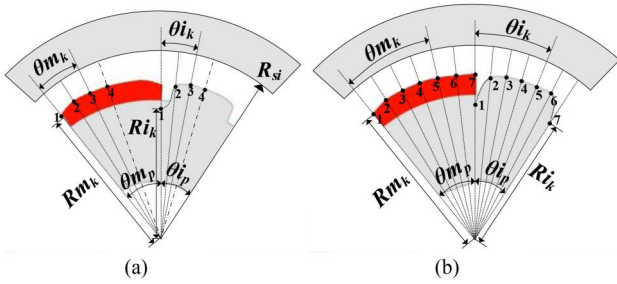


FIGURE 7 Models of two shaping methods. (a) Symmetrical, (b) Asymmetric.

3.2 | Optimisation results and analysis

CPPM and SPM machines with 12s8p and 9s6p as well as 12s10p and 12s14p are selected for demonstration, where the first two slot/pole number combinations belong to the first group and the last two slot/pole number combinations belong to the second group. The performances of CPPM and SPM models with symmetrical and asymmetric pole shapes, which will be denoted as Sym and Asym in the following text, are optimised for a combined objective of maximum torque and reduced torque ripple, as shown in Figures 8–11. The shaping optimisation with flexible rotor outline and pole arc span employs a Genetic Algorithm (GA) to explore rotor design parameters while the stator geometry remains fixed in the optimisation process with the key parameters listed in Table 4.

The optimisation results for two group machines produced by the GA are shown in Figures 8–11. To discover the potential of each shape of PM and iron poles, GA optimisation aims to obtain the Pareto frontiers rather than just finding an optimal case for each shape of the model. A total of over 40,000 combinations of rotor parameters are considered in GA optimisation to form the delicate Pareto frontiers, in each case by performing a two-dimensional FEM across one electrical cycle.

Figures 8 and 9 demonstrate the results for CPPM machines. Obviously, for the first group of machines, the frontiers

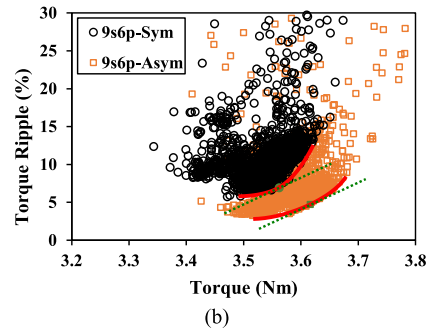
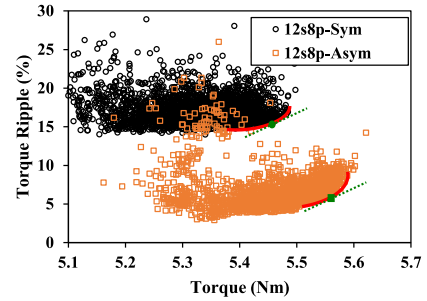


FIGURE 8 Pareto frontiers from multi-objective optimisation for Group 1 CPPM machines. (a) 12s8p, (b) 9s6p. CPPM, consequent pole permanent magnet.

of asymmetric models are much lower than those of symmetrical models in Figure 8, which means that the asymmetric pole shaping can result in a lower torque ripple. However, the frontiers for the second group of machines in Figure 9 are almost the same line, which means that the two pole shaping methods have a similar effect on torque ripple reduction. The results have validated the previous analyses.

Figures 10 and 11 demonstrate the results for SPM machines. It is clear that the frontiers of symmetrical and asymmetric models are almost the same line, which means that the two pole shaping methods have a similar effect on torque ripple reduction. The results also have validated the previous analyses.

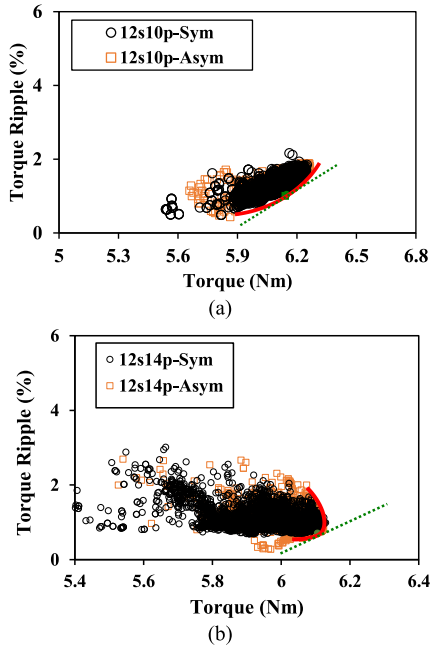


FIGURE 9 Pareto frontiers from multi-objective optimisation for Group 2 CPPM machines. (a) 12s10p, (b) 12s14p. CPPM, consequent pole permanent magnet.

To further investigate the specific electromagnetic performances of these pole-shaped models, some typical machines shown in the green points in Figures 8–11 are selected, which will be analysed in the following sections.

4 | COMPARISON AND ANALYSIS OF PERFORMANCES OF CPPM MACHINES

4.1 | Comparison and analysis of performances in group 1—CPPM machines having odd coil number per phase per submachine

For the first CPPM group machines, four typical machines that cover two pole shapes and two slot/pole number combinations as shown in green points in Figure 8 are identified and ultimately selected as representatives in the following analysis, where inevitable tradeoffs between average torque and torque ripple are necessary. The selected four machines will be denoted as 12s8p-Sym, 12s8p-Asym, 9s6p-Sym, and 9s6p-Asym, respectively, in the following parts. The rotor parameters for four selected models are listed in Table 5.

To provide useful baselines for comparison purposes, conventional CPPM machines which have plain magnet profiles without shaping are also considered and it will be denoted as Conv in the following text. The PM pole arc to pole pitch ratios of conventional models are set as 1.2 to maximise the average torque. The schematics of the optimised profiles together with their conventional CPPM counterparts are illustrated in Figure 12a–f.

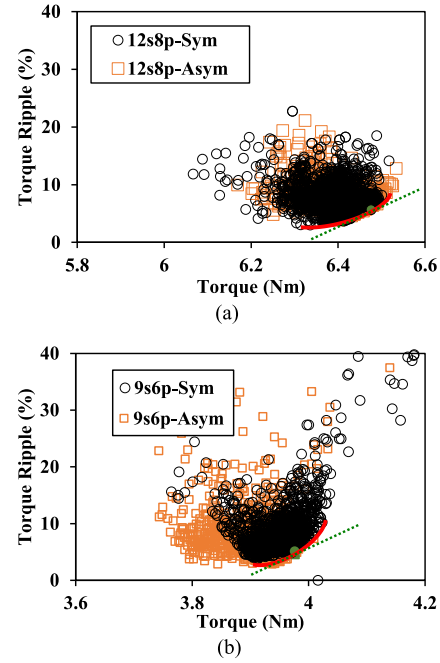


FIGURE 10 Pareto frontiers from multi-objective optimisation for Group 1 SPM machines. (a) 12s8p, (b) 9s6p. SPM, surface-mounted permanent magnet.

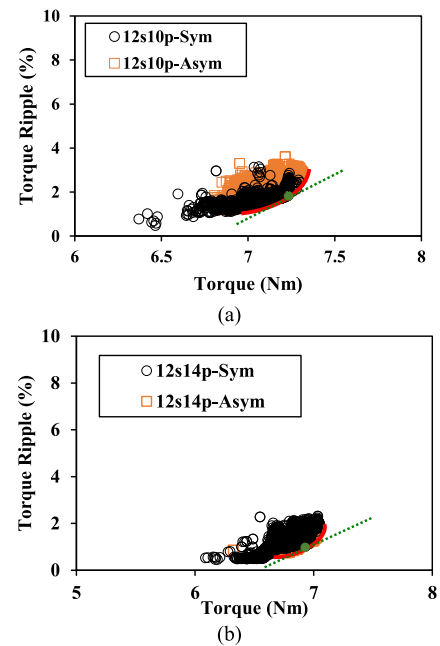


FIGURE 11 Pareto frontiers from multi-objective optimisation for Group 2 SPM machines. (a) 12s10p, (b) 12s14p. SPM, surface-mounted permanent magnet.

In the following part, FEM predicted performances of the CPPM machines detailed in Table 5 and Figure 12 under no-load and on-load conditions are analysed and compared.

4.1.1 | Open-circuit flux density and flux linkage

Neglecting the effect of slot openings for the time being, the no-load flux density distribution in air-gap for these CPPM machines and corresponding spectra are compared in Figure 13. It can be seen that the even order harmonics are evident in both 12s8p and 9s6p CPPM machines due to unbalanced features between PM and iron poles. Clearly, they can lead to the corresponding harmonics in coil flux linkages and phase winding flux linkages as shown in Figures 14 and 15. It can also be found that these pole-shaped models which have low torque ripples tend to exhibit lower amplitudes of harmonics in both flux density and flux linkage.

4.1.2 | Inductance

Figures 16 and 17 show the inductances for one coil and one phase winding, respectively. Obviously, due to iron saliency in CPPM rotor, the odd order harmonics exist in all the coil

inductances and winding inductances for all machines, which confirms the foregoing analyses.

4.1.3 | Cogging torque

Figure 18 shows the cogging torques for 12s8p and 9s6p machines. Supposing T_{ripple} is the peak-to-peak value for the cogging torques, as shown in Table 6, the pole-shaped CPPM machines tend to show lower cogging torques than those of their conventional counterparts. This can be attributed to the reduction in flux density harmonics for pole-shaped machines.

TABLE 4 Key design parameters of analysed machines

Parameter	Value	Unit
Stator outer radius	50	mm
Stator inner radius	28.5	mm
Axial length	50	mm
Air-gap length	1	mm
Stator yoke width	4.2	mm
Stator tooth width	8	mm
Stator turns per coil	46	-
Rated current	10	A_{pk}
Rated speed	400	r/min
Model of steel	35WW300	-
Model of magnet	N35	-
Remanence of magnet	1.2	T

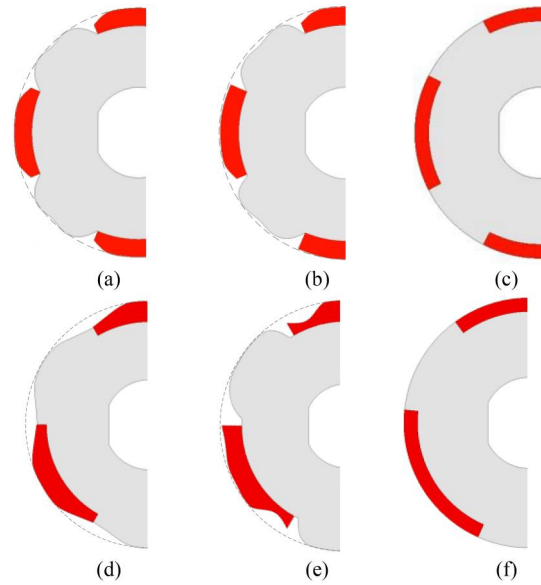


FIGURE 12 Optimised models for Group 1 CPPM machines. (a) 12s8p-Sym, (b) 12s8p-Asym, (c) 12s8p-Conv, (d) 9s6p-Sym, (e) 9s6p-Asym, and (f) 9s6p-Conv. CPPM, consequent pole permanent magnet.

TABLE 5 Rotor parameters for four optimised CPPM models

12s8p-Sym (mm)		12s8p-Asym (mm)		9s6p-Sym (mm)		9s6p-Asym (mm)					
Rm_1	25.93	Rm_1	25.93	Ri_1	23.55	Rm_1	25.06	Rm_1	25.97	Ri_1	21.27
Rm_2	27.28	Rm_2	27.35	Ri_2	26.54	Rm_2	26.11	Rm_2	24.66	Ri_2	25.27
Rm_3	27.49	Rm_3	27.50	Ri_3	27.25	Rm_3	27.47	Rm_3	27.49	Ri_3	27.11
Rm_4	27.44	Rm_4	27.49	Ri_4	26.89	Rm_4	27.45	Rm_4	27.30	Ri_4	27.46
Ri_1	23.94	Rm_5	27.49	Ri_5	27.45	Ri_1	24.95	Rm_5	27.32	Ri_5	27.49
Ri_2	26.62	Rm_6	27.39	Ri_6	27.15	Ri_2	25.66	Rm_6	26.71	Ri_6	27.08
Ri_3	27.41	Rm_7	27.32	Ri_7	22.97	Ri_3	27.09	Rm_7	27.23	Ri_7	20.70
Ri_4	27.08	θm_p	45.2°			Ri_4	27.43	θm_p	60.6°		
θm_p	44.9					θm_p	59.5°				

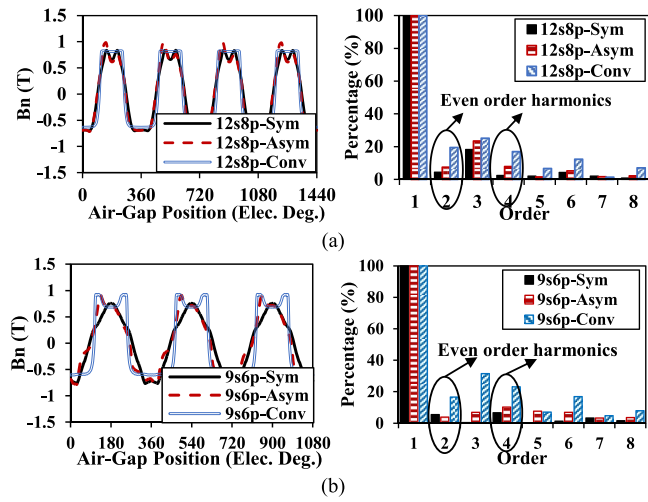


FIGURE 13 Air-gap flux density. (a) 12s8p, (b) 9s6p.

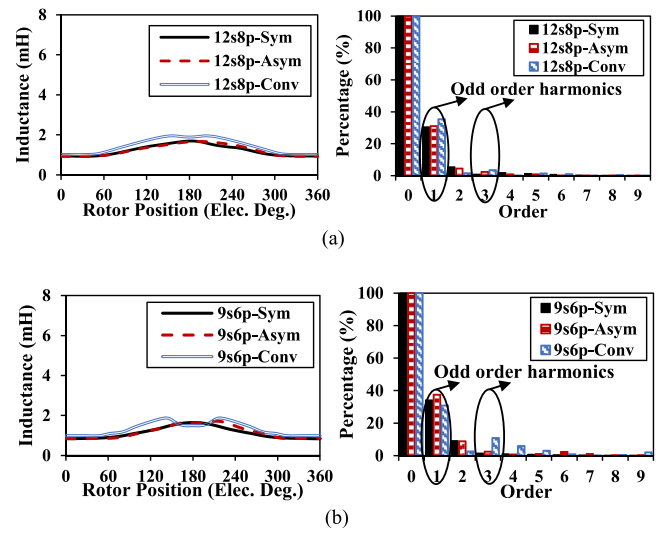


FIGURE 16 Inductances for one coil. (a) 12s8p, (b) 9s6p.

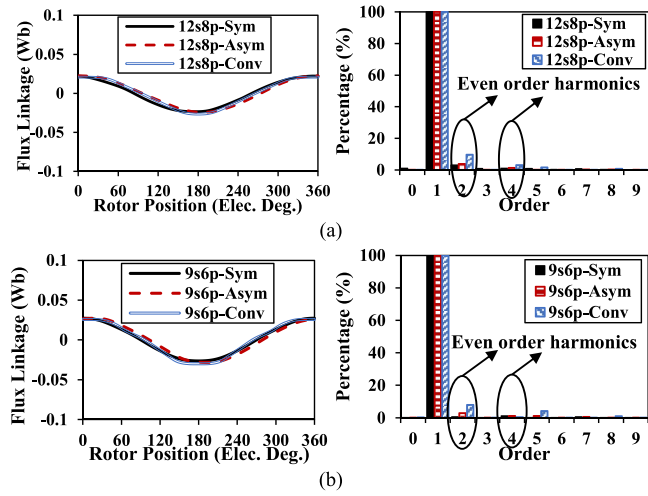


FIGURE 14 Open-circuit flux linkages for one coil. (a) 12s8p, (b) 9s6p.

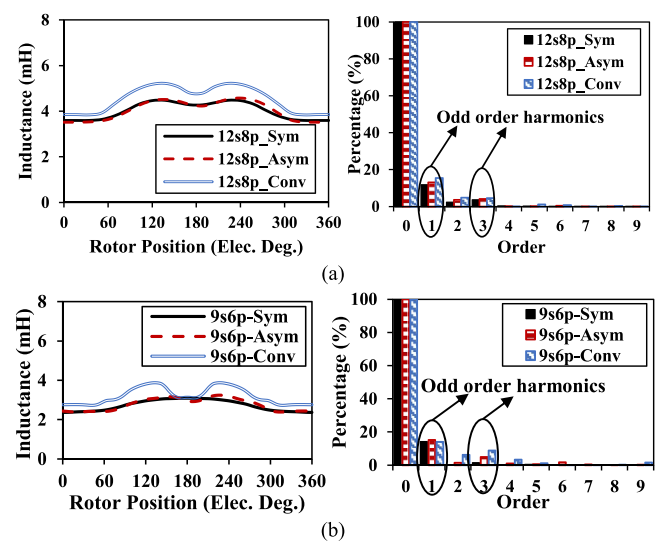


FIGURE 17 Inductances for one phase winding. (a) 12s8p, (b) 9s6p.

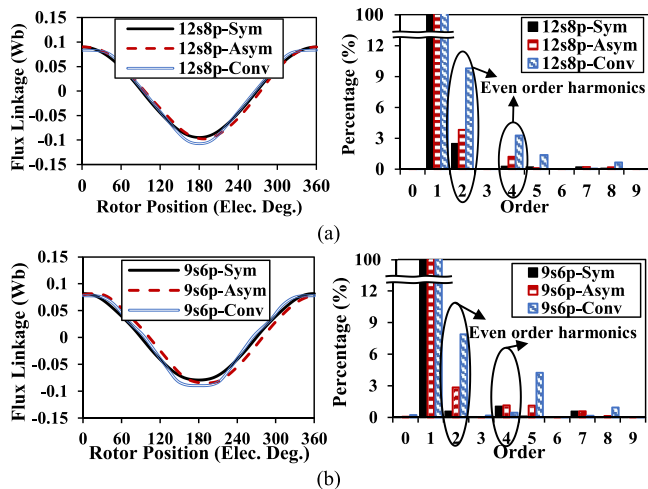


FIGURE 15 Open-circuit flux linkages for one phase winding. (a) 12s8p, (b) 9s6p.

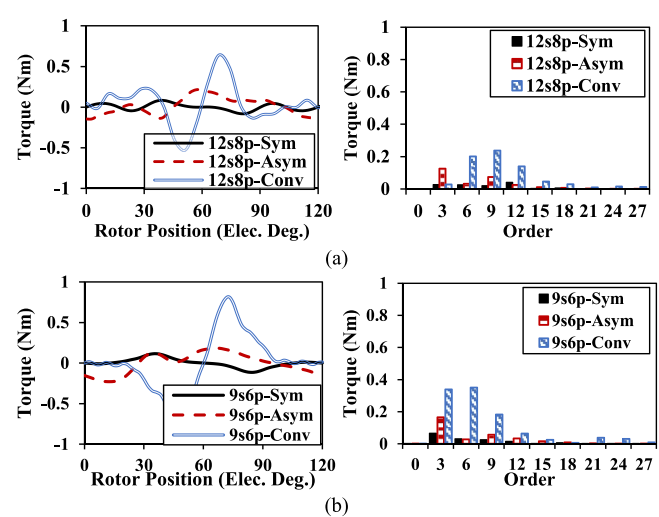


FIGURE 18 Cogging torque. (a) 12s8p, (b) 9s6p.

4.1.4 | Torque characteristics at rated load condition

Based on the average torque T_{avg} , the peak-to-peak torque T_{pp} and the volume of PM V_{PM} , the PM utilisation ratio η_{PM} and torque ripple T_{ripple} can be defined by:

$$\begin{aligned} \eta_{PM} &= T_{avg}/V_{PM} \\ T_{ripple} &= T_{pp}/T_{avg} \end{aligned} \quad (21)$$

The torque performances are compared in Table 7 and the torque waveforms are shown in Figure 19.

For these CPPM machines, the pole-shaped machines tend to have lower average torque than the conventional CPPM machine, which is largely a consequence of the almost same PM and iron pole arc spans for reduced even order harmonics.

In the case of torque ripple, it is evident that all machines have torque harmonic orders that are multiples of three and the asymmetric models have the lowest torque ripples among these machines. This is mainly because the harmonic torque components can be almost entirely counteracted, resulting in a reduced total torque ripple [13]. The results are consistent with the theoretical discussion in Section 3.

4.1.5 | Effect of l

Both average torques and torque ripples under different operating conditions are presented in Figure 20 where the grey dash line means the rated current condition. It can be observed that with increasing current (particularly beyond 10 A), the torque ripples of all the pole-shaped designs tend to increase but remain lower than those of their conventional

counterparts. This is mainly because the relative magnitudes of components of torque ripples are determined by the magnitude of the stator current.

When the injected current reduces from 10 A to 0, the torque ripples for pole-shaped machines show rising trends. This is largely a consequence of the relatively large contribution from cogging torque caused by flux density harmonics.

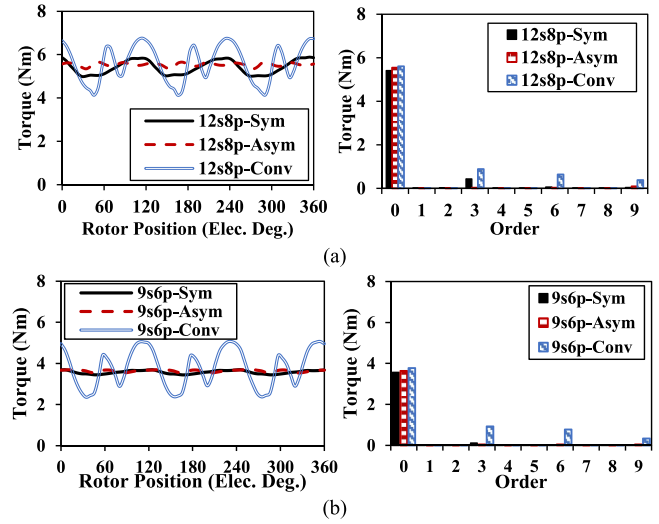


FIGURE 19 Rated torque. (a) 12s8p, (b) 9s6p.

TABLE 6 Summary of cogging torque of analysed machines

Machine	12s8p			9s6p		
	Sym	Asym	Conv	Sym	Asym	Conv
$T_{cogging}$ (mNm)	252	369	1166	228	413	1612

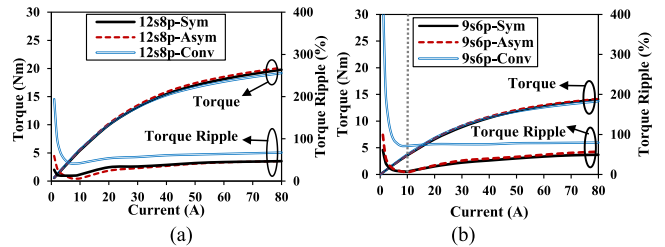


FIGURE 20 Torque characteristics under different loads. (a) 12s8p, (b) 9s6p.

TABLE 7 Torque characteristics and permanent magnet utilisation ratio comparison

Parameters	12s8p			9s6p		
	Sym	Asym	Conv	Sym	Asym	Conv
3^{rd} (Nm)	0.435	0.034	0.885	0.1126	0.047	0.9252
6^{th} (Nm)	0.066	0.032	0.635	0.0187	0.0414	0.7708
9^{th} (Nm)	0.044	0.092	0.385	0.0111	0.0438	0.3411
12^{th} (Nm)	0.023	0.031	0.253	0.0145	0.0122	0.1849
T_{pp} (Nm)	0.89	0.33	2.36	0.25	0.18	2.70
T_{avg} (Nm)	5.42	5.54	5.61	3.57	3.63	3.79
η_{PM} (Nm/m ³)	3.7×10^5	3.7×10^5	3.8×10^5	2.5×10^5	2.5×10^5	2.6×10^5
T_{ripple} (%)	16.4	5.9	42.1	7.0	4.9	71.4

The average torques are very similar for all three machines, and as a consequence of larger equivalent air-gap lengths, the lower armature effect of pole-shaped machines exhibits slightly enhanced overload capability.

4.1.6 | Radial force density

Since the vibration displacement is almost inversely proportional to the fourth power of the radial force spatial order, the lowest order radial force is critical to generate vibration, which is the greatest common divisor of slot number and pole number [16]. To evaluate the vibration performances of analysed machines, the lowest order (fourth for 12s8p and third for 9s6p) radial force densities are compared in Table 8. It is clear that compared with the conventional counterparts, the pole-shaped machines, including both symmetrical and asymmetric shaped machines, have lower amplitudes of radial force density which means that the pole shaping methods have the potential to reduce the vibration for CPPM machines in group 1.

4.2 | Comparison and analysis of performances in group 2—CPPM machines having even coil number per phase per submachine

For the second group CPPM machines, four typical machines, which are denoted as 12s10p-Sym, 12s10p-Asym, 12s14p-Sym,

and 12s14p-Asym, are selected as illustrated in green points in Figure 9. For comparison, conventional CPPM machines with plain PM and iron profiles without shaping are also analysed, which are denoted as 9s6p-Conv and 12s14p-Conv. The pole

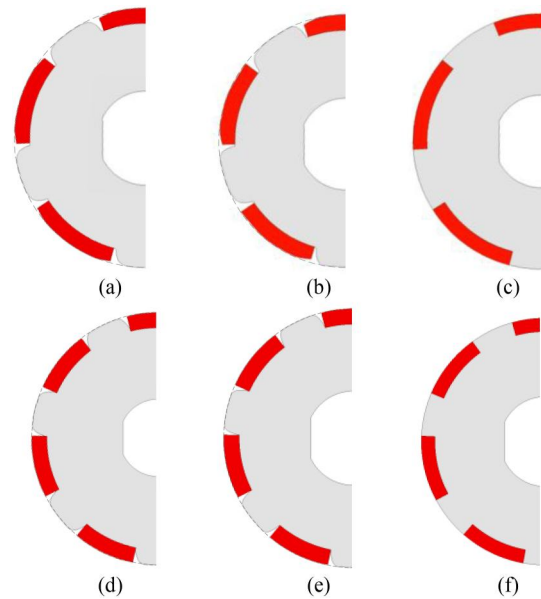


FIGURE 21 Optimised models for Group 2 CPPM machines. (a) 12s10p-Sym, (b) 12s10p-Asym, (c) 12s10p-Conv, (d) 12s14p-Sym, (e) 12s14p-Asym, and (f) 12s14p-Conv. CPPM, consequent pole permanent magnet.

TABLE 8 Main radial force densities of analysed machines

Force order	Amplitude (N/cm ²)					
	12s8p			9s6p		
	Sym	Asym	Conv	Sym	Asym	Conv
3	-	-	-	1.43×10^4	1.01×10^4	5.23×10^4
4	0.94×10^4	2.51×10^4	5.41×10^4	-	-	-

TABLE 9 Rotor parameters for four optimised CPPM models

12s10p-Sym (mm)		12s10p-Asym (mm)			12s14p-Sym (mm)		12s14p-Asym (mm)				
Rm_1	21.77	Rm_1	22.25	Ri_1	26.79	Rm_1	27.45	Rm_1	27.44	Ri_1	23.95
Rm_2	27.15	Rm_2	27.02	Ri_2	27.38	Rm_2	27.49	Rm_2	27.49	Ri_2	27.43
Rm_3	27.50	Rm_3	27.45	Ri_3	27.45	Rm_3	27.47	Rm_3	27.48	Ri_3	27.47
Rm_4	27.49	Rm_4	27.49	Ri_4	27.50	Rm_4	27.50	Rm_4	27.49	Ri_4	27.47
Ri_1	27.08	Rm_5	27.43	Ri_5	27.46	Ri_1	24.66	Rm_5	27.48	Ri_5	27.48
Ri_2	27.50	Rm_6	27.46	Ri_6	27.32	Ri_2	27.34	Rm_6	27.49	Ri_6	27.42
Ri_3	27.49	Rm_7	21.84	Ri_7	27.48	Ri_3	27.50	Rm_7	27.47	Ri_7	24.31
Ri_4	27.50	θm_p	39.4°			Ri_4	27.49	θm_p	28.5°		
θm_p	41.2°					θm_p	28.4°				

Abbreviation: CPPM, consequent pole permanent magnet.

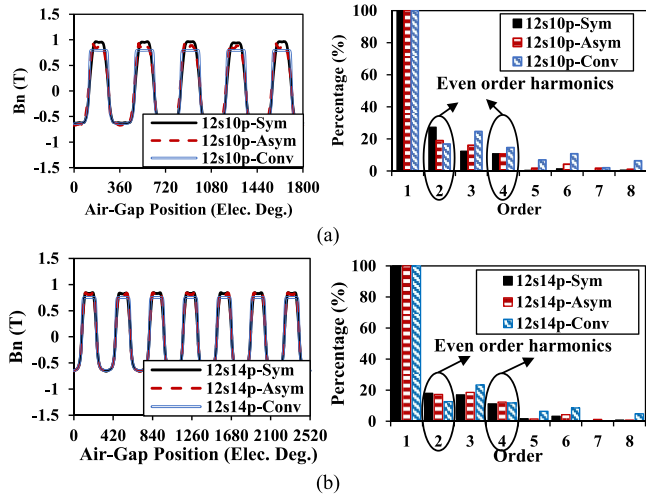


FIGURE 22 Air-gap flux density. (a) 12s10p, (b) 12s14p.

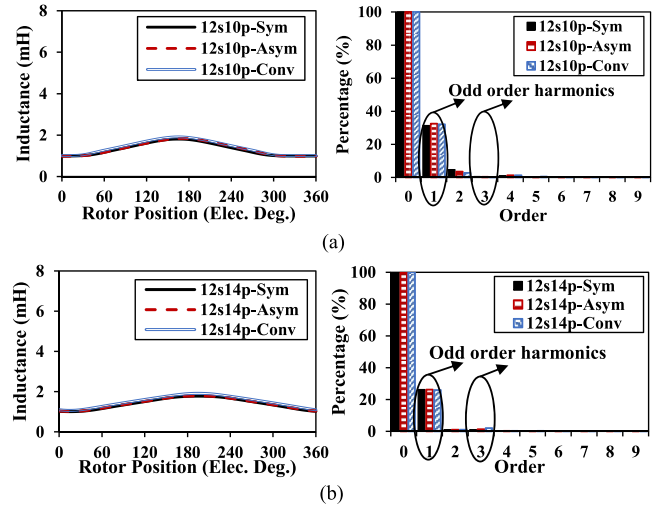


FIGURE 25 Inductances for one coil. (a) 12s10p, (b) 12s14p.

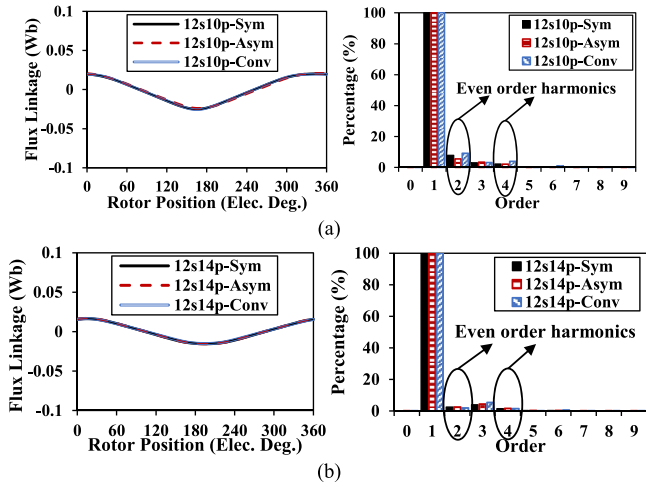


FIGURE 23 Open-circuit flux linkages for one coil. (a) 12s10p, (b) 12s14p.

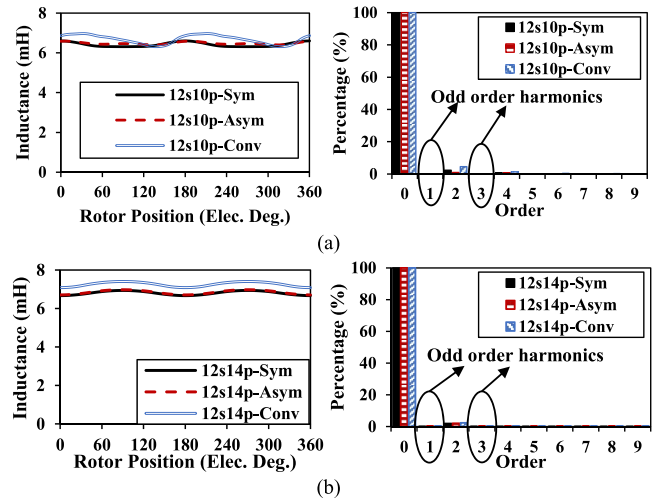


FIGURE 26 Inductances for one phase winding. (a) 12s10p, (b) 12s14p.

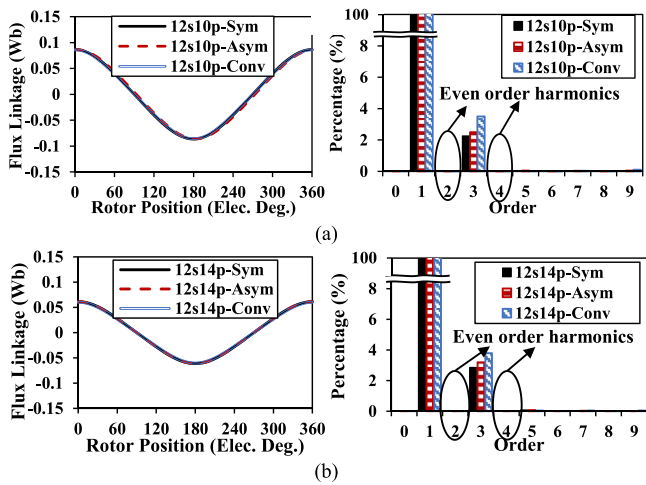


FIGURE 24 Open-circuit flux linkages for one phase winding. (a) 12s10p, (b) 12s14p.

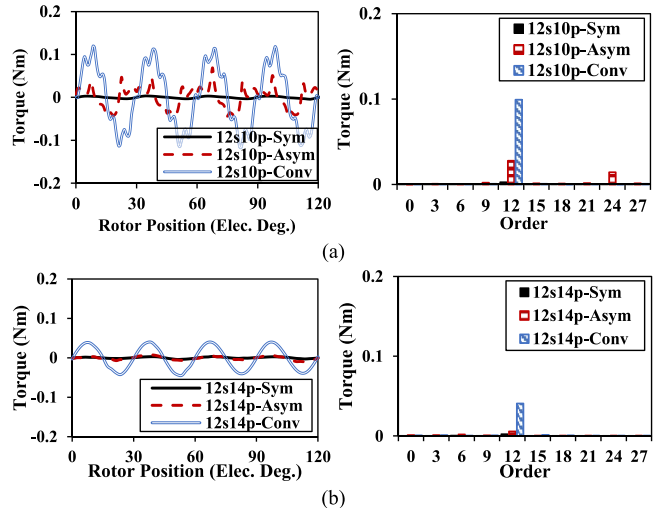


FIGURE 27 Cogging torque. (a) 12s10p, (b) 12s14p.

arc ratios of conventional models are set as 1.2 to maximise the average torque. The rotor geometry parameters for these machines are listed in Table 9 and the structures are presented in Figure 21. It is evident that the GA optimisation process has led to a larger PM pole arc span for optimised CPPM machines.

In the following part, FEM predicted performance of the CPPM machines detailed in Table 9 and Figure 21 under no-load and on-load conditions are analysed and compared.

4.2.1 | Open-circuit flux density and flux linkage

Open-circuit flux density distribution in air-gap for these CPPM machines and corresponding spectra are compared in Figure 22. Obviously, even order harmonics exist, leading to the corresponding harmonics in coil flux linkages as shown in Figure 23. However, in the phase winding flux linkages, even order harmonics are eliminated as shown in Figure 24.

4.2.2 | Inductance

Obviously, the odd order harmonics exist in all the coil inductances for all machines, Figure 25. However, in the phase winding inductances, the odd order harmonics are cancelled, Figure 26, which confirms the foregoing analyses.

4.2.3 | Cogging torque

Figure 27 illustrates the cogging torques for 12s10p and 12s14p machines and the peak-to-peak values are shown in Table 10. Lower cogging torques for pole-shaped CPPM machines can be found when compared with those of their conventional counterparts.

TABLE 10 Summary of cogging torque of analysed machines

Machine	12s10p			12s14p		
	Sym	Asym	Conv	Sym	Asym	Conv
T_{cogging} (mNm)	8	113	237	8	17	84

TABLE 11 Torque characteristics and permanent magnet utilisation ratio comparison

Parameters	12s10p			12s14p		
	Sym	Asym	Conv	Sym	Asym	Conv
6^{th} (Nm)	0.0359	0.0245	0.0528	0.0219	0.0215	0.037
12^{th} (Nm)	0.004	0.0227	0.144	0.0032	0.0039	0.0434
T_{pp} (Nm)	0.07	0.07	0.36	0.05	0.05	0.16
T_{avg} (Nm)	6.15	6.16	6.07	6.11	6.11	5.97
η_{PM} (Nm/m ³)	4.2×10^5	4.2×10^5	4.1×10^5	4.1×10^5	4.1×10^5	4.1×10^5
T_{ripple} (%)	1.2	1.2	5.9	0.8	0.9	2.6

4.2.4 | Torque characteristics at rated load condition

The torque performances are compared in Table 11 and the torque waveforms are shown in Figure 28. With the help of wider PM pole arcs and the air spaces adjacent to the sides of the magnets for reducing flux leakage, the pole-shaped machines can realise even higher average torque than their conventional counterpart and maintain high level PM utilisation ratios. In the case of torque ripple, it is evident that all the torque ripple orders for the second group CPPM machines are the multiple of 6 and the symmetrical and asymmetric models have similar levels of torque ripple. The results are consistent with the analysis in Section 3.

4.2.5 | Effect of load

Torque performances under different operating conditions are presented in Figure 29. It can be observed that when the current is beyond 10 A, the torque ripples of all the pole-shaped designs tend to maintain a low level. When the injected current is close to 0, the torque ripples for symmetrical

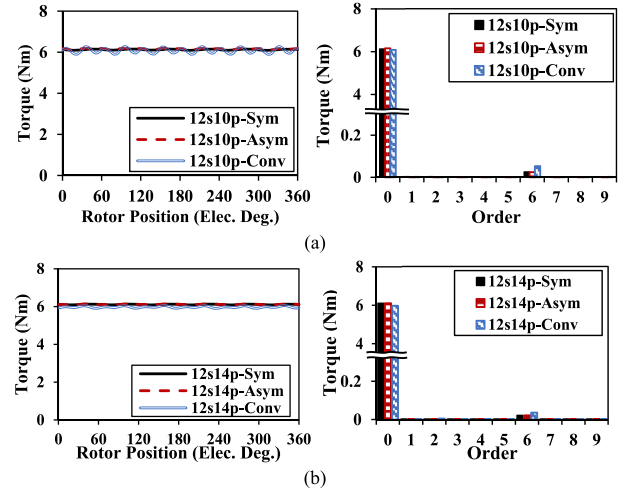


FIGURE 28 Rated torque. (a) 12s10p, (b) 12s14p.

pole-shaped machines are still low which is mainly because of their low cogging torques.

4.2.6 | Radial force density

The lowest order (the second for both 12s10p and 12s14p) radial force densities are compared in Table 12. It can be found that the pole-shaped machines, including both symmetrical and asymmetric shaped machines, tend to produce higher radial

force amplitudes which means that the pole shaping methods tend to increase the vibration for CPPM machines in group 2.

4.3 | Comparison

From the previous analyses, the characteristics of basic performances as well as the pole-shaped models for two groups of CPPM machines can be summarised and compared in Tables 13 and 14.

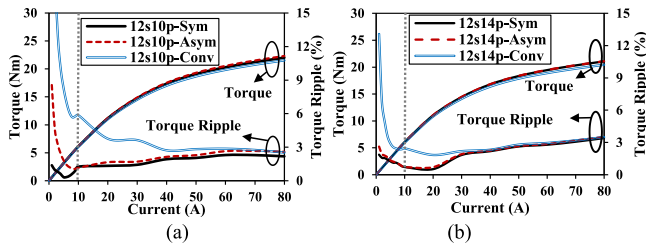


FIGURE 29 Torque characteristics under different loads. (a) 12s10p, (b) 12s14p.

5 | COMPARISON AND ANALYSIS OF PERFORMANCES OF SPM MACHINES

5.1 | Comparison and analysis of performances in group 1—SPM machines having odd coil number per phase per submachine

For the first group SPM machines, four typical machines, which are denoted as 12s8p-Sym, 12s8p-Asym, 9s6p-Sym, and

TABLE 12 Main radial force densities of analysed machines

Force order	Amplitude (N/cm ²)					
	12s10p			12s14p		
	Sym	Asym	Conv	Sym	Asym	Conv
2	7.44×10^3	4.66×10^3	0.96×10^3	4.85×10^3	4.41×10^3	0.12×10^3

TABLE 13 Characteristics of basic performance for two groups of CPPM Machines

Machine	Group 1 for example, 12s8p, 9s6p, 9s8p etc.	Group 2 for example, 12s10p, 12s14p, 6s10p etc.
Flux density in air-gap	With even order harmonics	
Coil flux linkage	With even order harmonics	
Phase winding flux linkage	With even order harmonics	Without even order harmonics
Coil inductance	With odd order harmonics	
Winding inductance	With odd order harmonics	Without odd order harmonics
Torque ripple	Harmonics orders are multiples of 3	Harmonics orders are multiples of 6

Abbreviation: CPPM, consequent pole permanent magnet.

TABLE 14 Characteristics of pole-shaped models for two groups of CPPM machines

Machine	Group 1 for example, 12s8p, 9s6p, 9s8p etc.	Group 2 for example, 12s10p, 12s14p, 6s10p etc.
Pole shaping method	Asymmetric pole shaping can result in a much lower torque ripple than symmetrical pole shaping	Symmetrical pole shaping method can achieve a similar level of torque ripple as that of asymmetric method but with lower optimisation complexity
Pole arc width	PM and iron pole arcs need to be almost identical	PM pole arc should be larger than iron pole arc
Overload capability	Overload capabilities for shaped machines are all improved slightly	

Abbreviation: CPPM, consequent pole permanent magnet.

TABLE 15 Rotor parameters for four pole-shaped SPM models

12s8p-Sym (mm)		12s8p-Asym (mm)		9s6p-Sym (mm)		9s6p-Asym (mm)					
Rm_1	23.86	Rm_1	23.19	Ri_1	24.19	Rm_1	22.96	Rm_1	24.12	Ri_1	21.58
Rm_2	26.89	Rm_2	26.39	Ri_2	27.15	Rm_2	25.31	Rm_2	25.43	Ri_2	25.00
Rm_3	27.47	Rm_3	27.46	Ri_3	27.47	Rm_3	27.39	Rm_3	27.12	Ri_3	27.20
Rm_4	27.27	Rm_4	27.12	Ri_4	27.33	Rm_4	27.25	Rm_4	27.20	Ri_4	27.01
Ri_1	23.71	Rm_5	27.37	Ri_5	27.45	Ri_1	22.95	Rm_5	27.16	Ri_5	27.42
Ri_2	27.03	Rm_6	27.24	Ri_6	26.90	Ri_2	25.14	Rm_6	25.37	Ri_6	25.83
Ri_3	27.46	Rm_7	25.04	Ri_7	25.95	Ri_3	27.38	Rm_7	23.50	Ri_7	22.73
Ri_4	27.35	θm_p	44.44			Ri_4	27.22	θm_p	60.42		
θm_p	44.81					θm_p	60.58				

Abbreviation: SPM, surface-mounted permanent magnet.

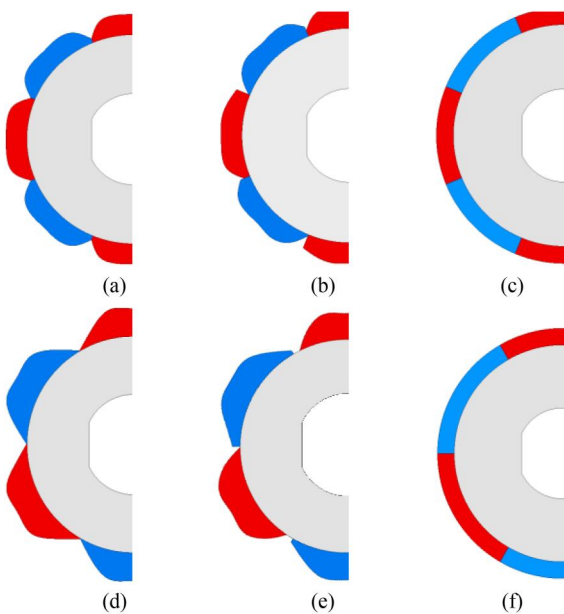


FIGURE 30 Optimised models for Group 1—SPM machines. (a) 12s8p-Sym, (b) 12s8p-Asym, (c) 12s8p-Conv, (d) 9s6p-Sym, (e) 9s6p-Asym, and (f) 9s6p-Conv. SPM, surface-mounted permanent magnet.

9s6p-Asym, are selected as illustrated in green points in Figure 10. For comparison, conventional SPM machines with plain PM profiles without shaping and equal north and south pole widths are also analysed, which are denoted as 12s8p-Conv and 9s6p-Conv. The rotor geometry parameters for these machines are listed in Table 15 and the structures are presented in Figure 30. It is evident that the GA optimisation process has led to almost equal north and south pole widths.

The flux densities, flux linkages, inductances, torque performances, and radial force densities for these six machines are shown in Figures 31–38, Tables 16–18. It is obvious that the conventional SPM machine with equal north and south pole widths can eliminate the additional harmonics in flux densities, flux linkages, and inductances, while the pole-shaped machines tend to have those harmonics. Similar to CPPM counterparts,

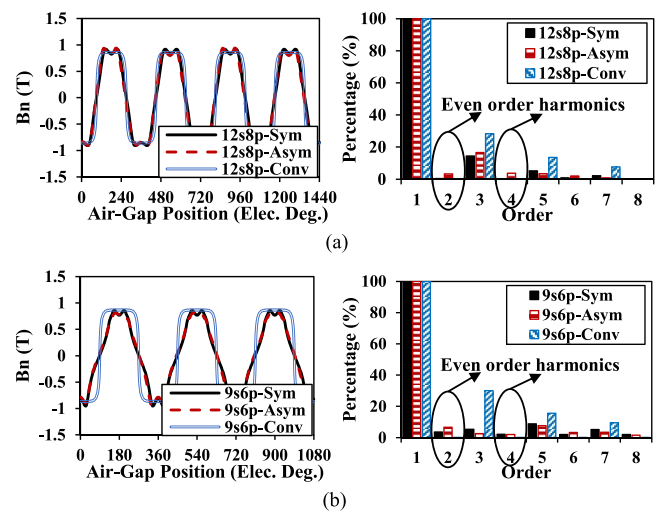


FIGURE 31 Air-gap flux density. (a) 12s8p, (b) 9s6p.

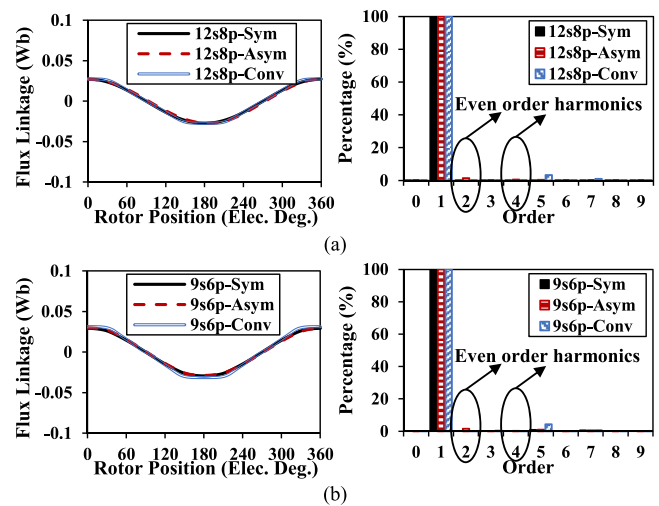


FIGURE 32 Open-circuit flux linkages for one coil. (a) 12s8p, (b) 9s6p.

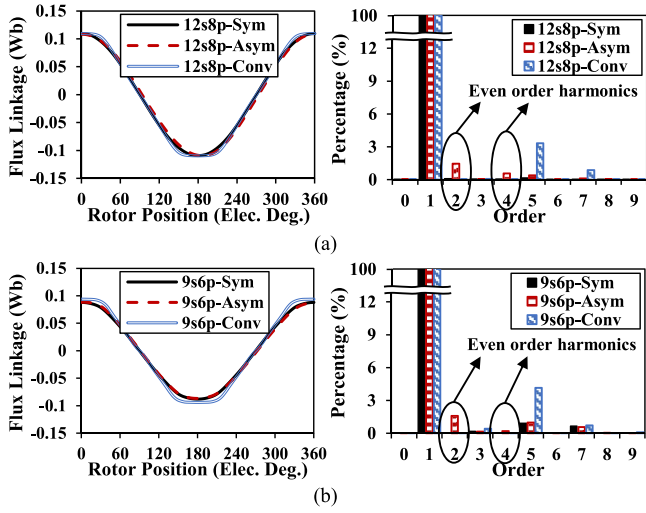


FIGURE 33 Open-circuit flux linkages for one phase winding. (a) 12s8p, (b) 9s6p.

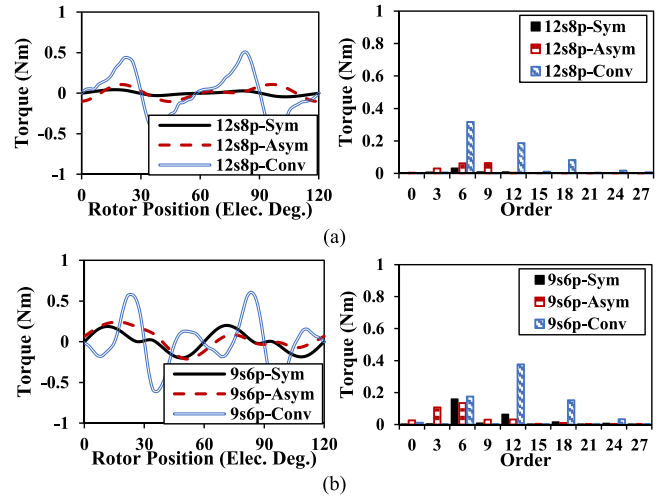


FIGURE 36 Cogging torque. (a) 12s8p, (b) 9s6p.

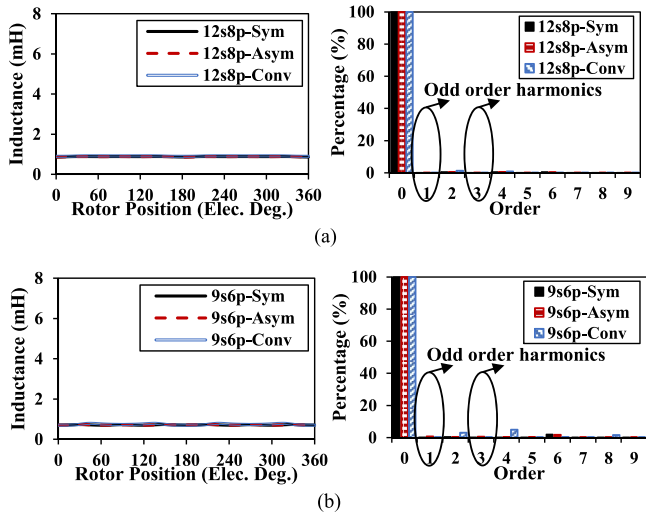


FIGURE 34 Inductances for one coil. (a) 12s8p, (b) 9s6p.

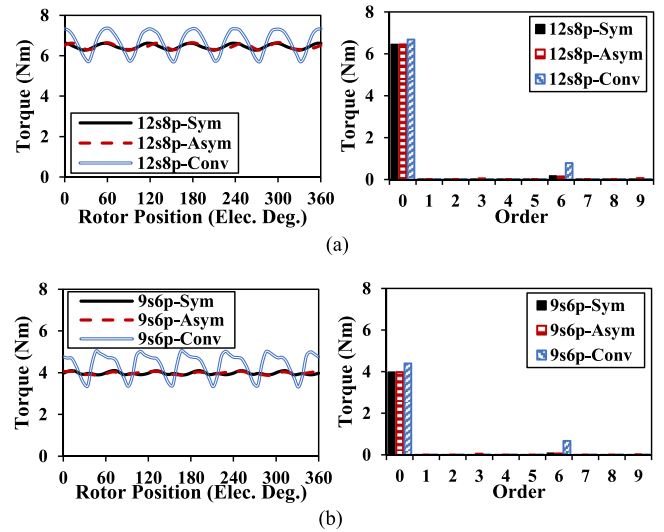


FIGURE 37 Rated torque. (a) 12s8p, (b) 9s6p.

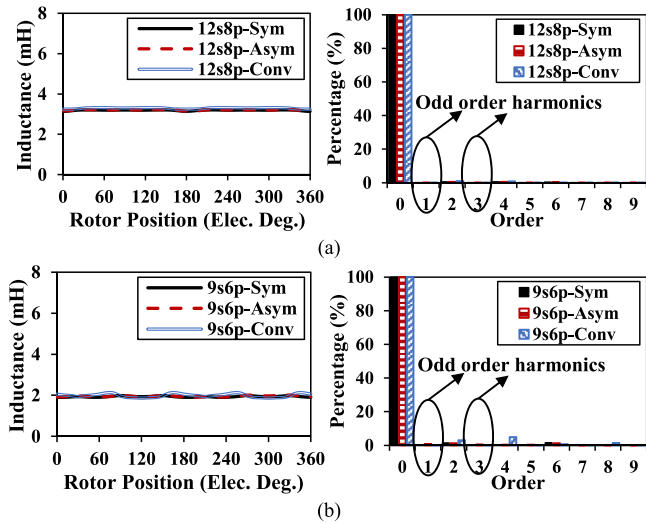


FIGURE 35 Inductances for one phase winding. (a) 12s8p, (b) 9s6p.

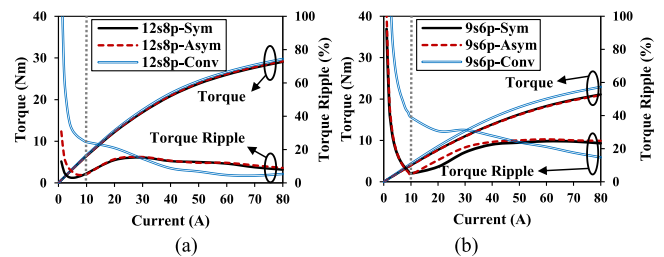


FIGURE 38 Torque characteristics under different loads. (a) 12s8p, (b) 9s6p.

the even order harmonics in air-gap flux densities can produce corresponding harmonics in winding flux linkages, which will lead to odd order torque ripples. However, due to the objective of low torque ripple in optimisation, all the harmonics are low enough. It can also be found that symmetrical and asymmetric

pole-shaped machines have similar torque ripple levels, which confirms the analysis in Section 3. In addition, the pole shaping methods tend to increase the radial force and thus vibration for SPM machines in group 1.

5.2 | Comparison and analysis of performances in group 2—SPM machines having even coil number per phase per submachine

For the second group SPM machines, four typical machines as shown in green points in Figure 11 are selected with their structures and parameters demonstrated in Figure 39 and Table 19. Similar to the first group SPM machines, the optimised models have almost same north and south pole widths, which can reduce the unbalance between two poles. Also, conventional SPM with equal north and south pole arc widths are also selected for comparison.

The flux densities, flux linkages, inductances, and torque performances for these six machines are shown in Figures 40–47 and Tables 20 and 21. Similar to the first group SPM

machines, the pole-shaped machines tend to have additional flux density harmonics. But these harmonics can be eliminated in winding flux linkages, which will not lead to odd order torque ripples. Also, symmetrical and asymmetric pole-shaped

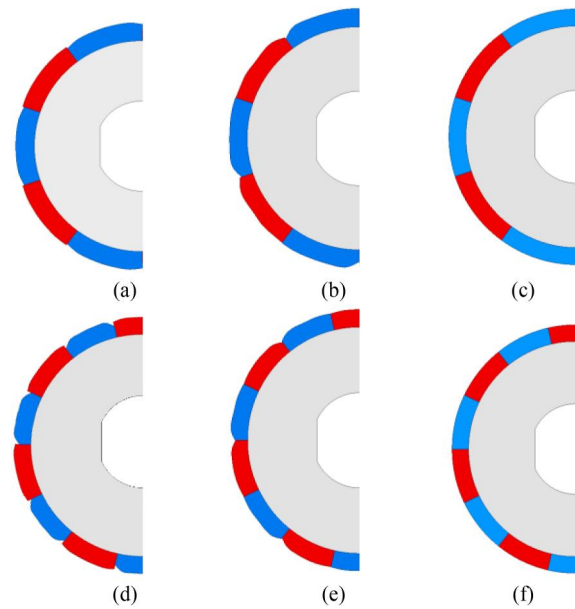


FIGURE 39 Optimised models for Group 2—SPM machines. (a) 12s10p-Sym, (b) 12s10p-Asym, (c) 12s10p-Conv, (d) 12s14p-Sym, (e) 12s14p-Asym, and (f) 12s14p-Conv. SPM, surface-mounted permanent magnet.

TABLE 16 Summary of cogging torque of analysed machines

Machine	12s8p			9s6p		
	Sym	Asym	Conv	Sym	Asym	Conv
T_{cogging} (mNm)	88	210	965	397	453	1241

TABLE 17 Torque characteristics and permanent magnet utilisation ratio comparison

Parameters	12s8p			9s6p		
	Sym	Asym	Conv	Sym	Asym	Conv
3^{rd} (Nm)	0.0088	0.0492	0.006	0.0023	0.0514	0.0024
6^{th} (Nm)	0.1708	0.1452	0.7784	0.0751	0.0594	0.6686
9^{th} (Nm)	0.0121	0.0607	0.0045	0.0056	0.0186	0.0039
12^{th} (Nm)	0.0074	0.0068	0.1495	0.0474	0.0216	0.338
T_{pp} (Nm)	0.36	0.35	1.66	0.19	0.19	1.71
T_{avg} (Nm)	6.46	6.45	6.69	3.97	3.98	4.40
η_{PM} (Nm/m ³)	2.2×10^5	2.1×10^5	2.3×10^5	1.3×10^5	1.3×10^5	1.5×10^5
T_{ripple} (%)	5.6	5.5	24.7	4.9	4.7	38.9

TABLE 18 Main radial force densities of analysed machines

Force order	Amplitude (N/cm ²)					
	12s8p			9s6p		
	Sym	Asym	Conv	Sym	Asym	Conv
3	-	-	-	1.02×10^3	1.77×10^3	0.88×10^3
4	0.13×10^4	1.59×10^4	0.04×10^4	-	-	-

TABLE 19 Rotor parameters for four pole-shaped SPM models

12s10p-Sym (mm)		12s10p-Asym (mm)		12s14p-Sym (mm)		12s14p-Asym (mm)					
Rm_1	27.05	Rm_1	26.09	Ri_1	27.40	Rm_1	26.22	Rm_1	26.49	Ri_1	27.26
Rm_2	27.48	Rm_2	27.43	Ri_2	27.35	Rm_2	27.43	Rm_2	27.38	Ri_2	27.43
Rm_3	27.49	Rm_3	27.41	Ri_3	27.45	Rm_3	27.45	Rm_3	27.50	Ri_3	27.49
Rm_4	27.49	Rm_4	27.34	Ri_4	27.26	Rm_4	27.48	Rm_4	27.37	Ri_4	27.48
Ri_1	27.40	Rm_5	27.36	Ri_5	27.37	Ri_1	27.15	Rm_5	27.44	Ri_5	27.39
Ri_2	27.50	Rm_6	27.48	Ri_6	27.34	Ri_2	27.50	Rm_6	27.43	Ri_6	27.21
Ri_3	27.49	Rm_7	27.47	Ri_7	26.44	Ri_3	27.47	Rm_7	27.31	Ri_7	26.29
Ri_4	27.50	θm_p	35.43			Ri_4	27.48	θm_p	25.84		
θm_p	34.52					θm_p	26.42				

Abbreviation: SPM, surface-mounted permanent magnet.

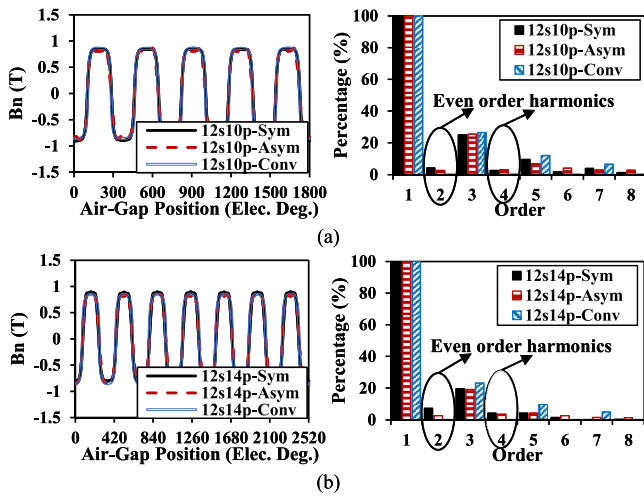


FIGURE 40 Air-gap flux density. (a) 12s10p, (b) 12s14p.

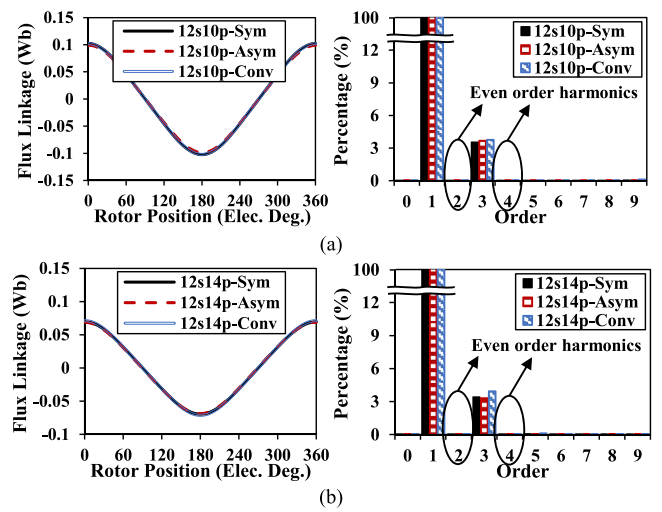


FIGURE 42 Open-circuit flux linkages for one phase winding. (a) 12s10p, (b) 12s14p.

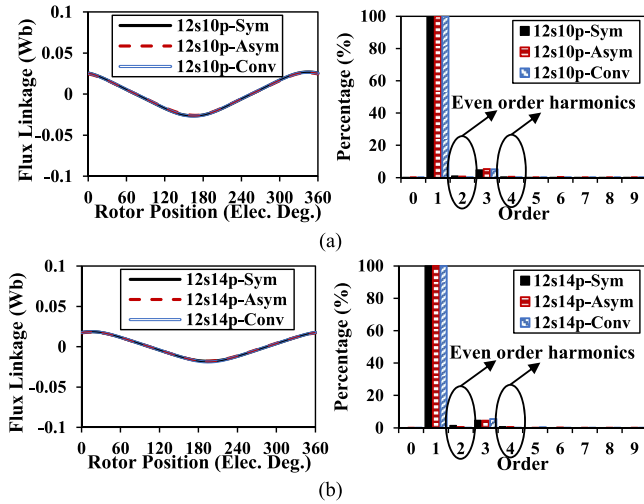


FIGURE 41 Open-circuit flux linkages for one coil. (a) 12s10p, (b) 12s14p.

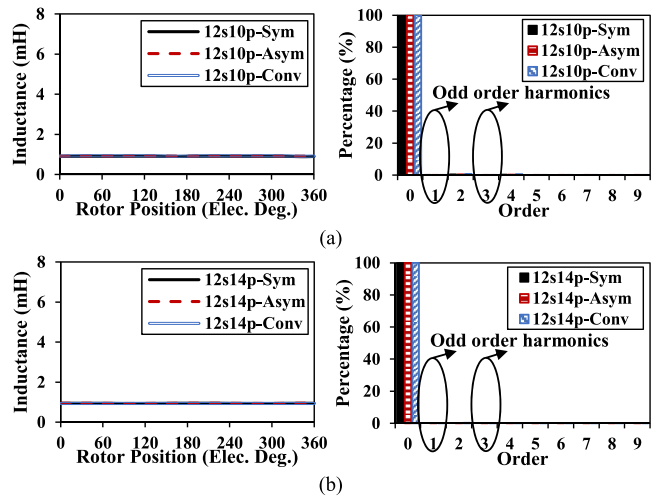


FIGURE 43 Inductances for one coil. (a) 12s10p, (b) 12s14p.

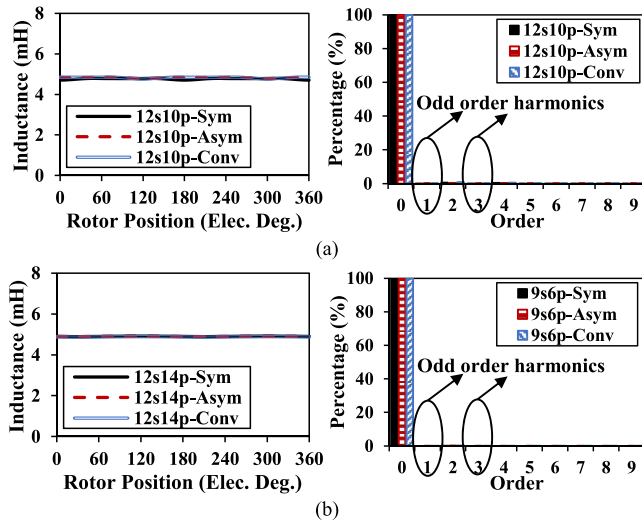


FIGURE 44 Inductances for one phase winding. (a) 12s10p, (b) 12s14p.

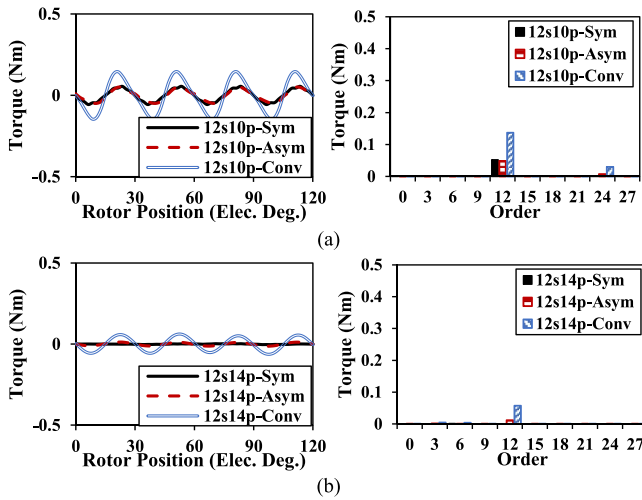


FIGURE 45 Cogging torque. (a) 12s10p, (b) 12s14p.

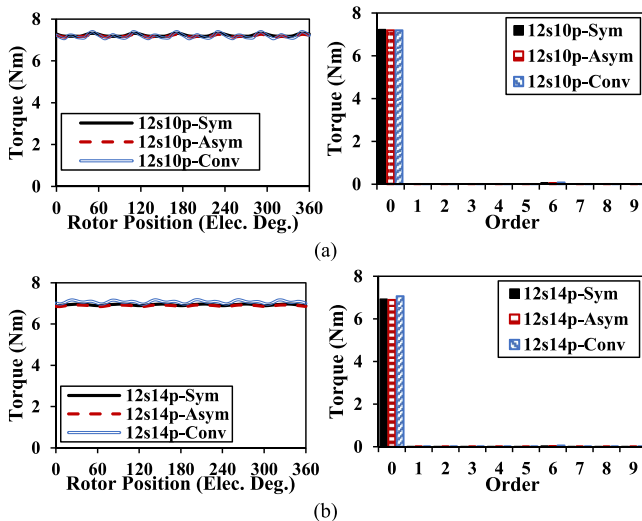


FIGURE 46 Rated torque. (a) 12s10p, (b) 12s14p.

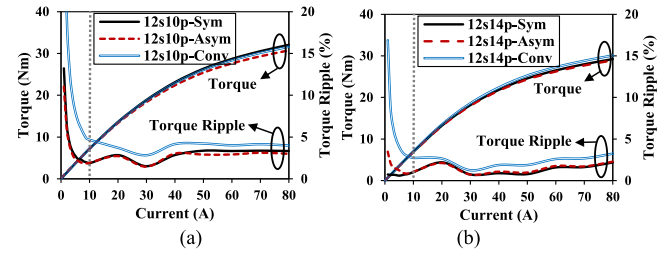


FIGURE 47 Torque characteristics under different loads. (a) 12s10p, (b) 12s14p.

TABLE 20 Summary of cogging torque of analysed machines

Machine	12s10p			12s14p		
	Sym	Asym	Conv	Sym	Asym	Conv
T_{cogging} (mNm)	112	100	292	5	26	123

machines have similar torque ripple levels, which confirms the analysis in Section 3. In addition, the pole shaping methods tend to increase the radial force and thus vibration for SPM machines in group 2 as shown in Table 22.

5.3 | Comparison

From the previous analysis, the characteristics of basic performances as well as the pole-shaped models for two groups of SPM machines can be summarised in Tables 23 and 24.

6 | COMPARISONS BETWEEN CPPM AND SPM MACHINES

Torque ripple T_{ripple} , average torque T_{avg} , torque density T_{den} (ratio of T_{avg} to overall machine volume), and PM utilisation ratio η_{PM} of CPPM and SPM machines are compared in Table 25. From Table 25, it can be seen that the torque ripples of conventional CPPM machines are significantly higher than those of SPM counterparts in the first group. It can also be found that for the first group of CPPM machines, the asymmetric pole shaping method can obviously contribute to lower torque ripple than symmetrical pole shaping method. But these two shaping methods have similar capabilities in torque ripple reduction for other machines. Besides, the CPPM machines have a little bit lower average torque than their SPM counterparts. Since all machines have identical stator outer radii and stack lengths, the torque densities for them show the same trend as the average torque. However, the PM utilisation ratios of CPPM machines are much higher than those of SPM counterparts for both conventional and pole-shaped machines.

Based on the above analyses, the characteristics of CPPM and SPM machines in terms of air-gap flux density, winding flux linkage, inductance, torque ripples, and effects of pole shaping machines are compared Table 26.

TABLE 21 Torque characteristics and permanent magnet utilisation ratio comparison

Parameters	12s10p			12s14p		
	Sym	Asym	Conv	Sym	Asym	Conv
6^{th} (Nm)	0.0678	0.0522	0.0783	0.0343	0.0344	0.0582
12^{th} (Nm)	0.0219	0.027	0.1101	0.004	0.009	0.0551
T_{pp} (Nm)	0.14	0.14	0.34	0.07	0.08	0.22
T_{avg} (Nm)	7.23	7.19	7.20	6.93	6.89	7.07
η_{PM} (Nm/m ³)	2.3×10^5	2.4×10^5	2.4×10^5	2.4×10^5	2.4×10^5	2.4×10^5
T_{ripple} (%)	1.9	1.9	4.7	1.1	1.1	3.0

TABLE 22 Main radial force densities of analysed machines

Force order	Amplitude (N/cm ²)					
	12s10p			12s14p		
	Sym	Asym	Conv	Sym	Asym	Conv
2	0.62×10^3	0.50×10^3	0.43×10^3	1.33×10^3	1.31×10^3	0.80×10^3

TABLE 23 Characteristics of basic performance for SPM machines

Machine	With unequal pole widths		With equal pole widths	
	Group 1	Group 2	Group 1	Group 2
Flux density in air-gap	With even order harmonics		Without even order harmonics	
Coil flux linkage	With even order harmonics		Without even order harmonics	
Winding flux linkage	With even order harmonics		Without even order harmonics	
Coil inductance	Without odd order harmonics		Without odd order harmonics	
Winding inductance	Without odd order harmonics		Without odd order harmonics	
Torque ripple	Harmonics orders are multiples of 3		Harmonics orders are multiples of 6	

Abbreviation: SPM, surface-mounted permanent magnet.

TABLE 24 Characteristics of pole-shaped models for two groups of SPM machines

Machine	First group for example, 12s8p, 9s6p, 9s8p etc.	Second group for example, 12s10p, 12s14p, 6s10p etc.
Pole shaping method	Symmetrical pole shaping method can achieve a similar level of torque ripple as that of asymmetric method but with lower optimisation complexity	
Pole arc width	North and south pole arc need to be almost identical	

Abbreviation: SPM, surface-mounted permanent magnet.

7 | EXPERIMENTAL VERIFICATION AND DISCUSSION

Based on the parameters listed in Table 4, two stators with 12-slot and 6 CPPM rotors with both 8-pole and 10-pole are manufactured as shown in Figure 48. It should be noted that

the only difference for stators in Figure 48a is the winding connection due to different poles numbers. The models for steel and magnet are 35WW300 and N35 as well as their curves are illustrated in Figure 49. The on-load torque is tested on the dynamic platform, Figure 50a, while the inductances are measured on the static platform, Figure 50b.

TABLE 25 Quantitative torque characteristics comparisons between CPPM and SPM machines

Machine			T_{ripple} (%)	T_{avg} (Nm)	T_{den} (Nm/m ³)	η_{PM} (Nm/m ³)
CPPM First group	12s8p	Sym	16.4	5.42	1.4×10^4	3.7×10^5
		Asym	5.9	5.54	1.4×10^4	3.7×10^5
		Conv	42.1	5.61	1.4×10^4	3.8×10^5
	9s6p	Sym	7	3.57	9.1×10^3	2.5×10^5
		Asym	4.9	3.63	9.2×10^3	2.5×10^5
		Conv	71.4	3.79	9.7×10^3	2.6×10^5
CPPM Second group	12s10p	Sym	1.2	6.15	1.6×10^4	4.2×10^5
		Asym	1.2	6.16	1.6×10^4	4.2×10^5
		Conv	5.9	6.07	1.5×10^4	4.1×10^5
	12s14p	Sym	0.8	6.11	1.6×10^4	4.1×10^5
		Asym	0.9	6.11	1.6×10^4	4.1×10^5
		Conv	2.6	5.97	1.5×10^4	4.1×10^5
SPM First group	12s8p	Sym	5.6	6.46	1.6×10^4	2.2×10^5
		Asym	5.5	6.45	1.6×10^4	2.1×10^5
		Conv	24.7	6.69	1.7×10^4	2.3×10^5
	9s6p	Sym	4.9	3.97	1.0×10^4	1.3×10^5
		Asym	4.7	3.98	1.0×10^4	1.3×10^5
		Conv	38.9	4.4	1.1×10^4	1.5×10^5
SPM Second group	12s10p	Sym	1.9	7.23	1.8×10^4	2.3×10^5
		Asym	1.9	7.19	1.8×10^4	2.4×10^5
		Conv	4.7	7.2	1.8×10^4	2.4×10^5
	12s14p	Sym	1.1	6.93	1.8×10^4	2.4×10^5
		Asym	1.1	6.89	1.8×10^4	2.4×10^5
		Conv	3	7.07	1.8×10^4	2.4×10^5

Abbreviations: CPPM, consequent pole permanent magnet; SPM, surface-mounted permanent magnet.

TABLE 26 Characteristics comparison of CPPM and SPM machines

Machine	CPPM	SPM
First group	<ul style="list-style-type: none"> • Even order harmonics in air-gap flux density can produce corresponding harmonics in winding flux linkage. • Odd order harmonics in inductance cannot be eliminated. • Torque ripple harmonics orders are multiples of 3. • Compared with symmetrical pole shaping method, asymmetric pole shaping method can contribute to lower torque ripple. 	<ul style="list-style-type: none"> • Even order harmonics in air-gap flux density can produce corresponding harmonics in winding flux linkage. • There are no harmonics in inductance. • Torque ripple harmonics orders are multiples of 3 with unequal north and south pole widths, while they are 6 with equal pole widths. • Symmetrical and asymmetric pole shaping methods have similar capabilities in torque ripple reduction.
Second group	<ul style="list-style-type: none"> • Even order harmonics in winding flux linkage can be eliminated due to cancelation effect of coil connections. • There are no odd order harmonics in inductance. • Torque ripple harmonics orders are multiples of 6. • Symmetrical and asymmetric pole shaping methods have similar capabilities in torque ripple reduction. 	

Abbreviations: CPPM, consequent pole permanent magnet; SPM, surface-mounted permanent magnet.

TABLE 27 Torque performances comparisons for prototypes

Machine		Torque (Nm)		Torque ripple (%)	
		Measured	Predicted	Measured	Predicted
12s8p	Sym	5.41	5.42	16.8	16.4
	Asym	5.47	5.54	10.4	5.9
	Conv	5.68	5.61	35.7	42.1
12s10p	Sym	6.12	6.15	2.6	1.2
	Asym	6.06	6.16	3.5	1.2
	Conv	6.18	6.07	5.2	5.9

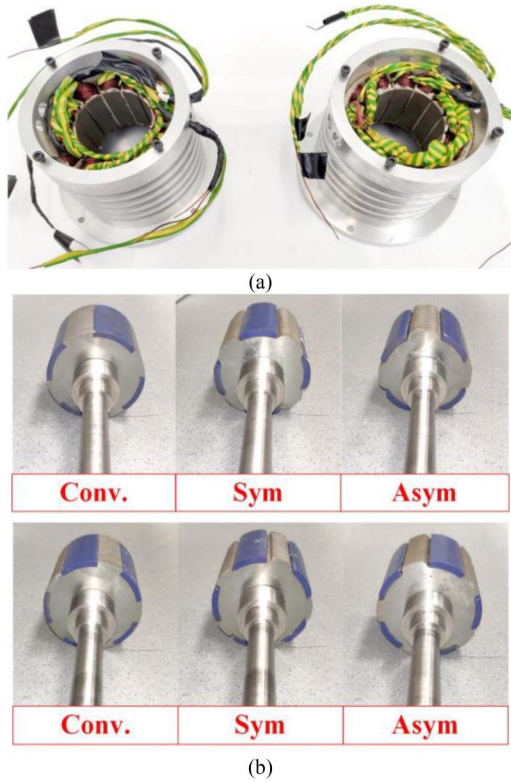


FIGURE 48 Manufactured prototypes with and without shaping. (a) Stators (left: 8-pole, right: 10-pole), (b) Rotors (above: 8-pole, bottom: 10-pole).

Although the manufacturing cost will be relatively higher for the low volume prototyping of pole-shaped CPPM machines, the cost will be almost the same as conventional CPPM machines in mass production since the increased cost of mould can be minor [33].

7.1 | Back EMF

For the phase back EMF tests, a DC motor is used to drive the rotor of the prototype machine. Figure 51 shows the measured and predicted phase back EMFs with the rotor position at

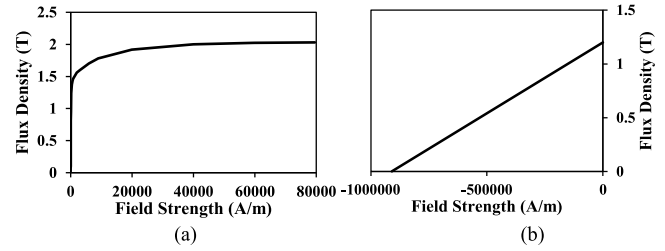


FIGURE 49 B-H curves for steel and magnet. (a) Steel—35WW400, (b) Magnet—N35.

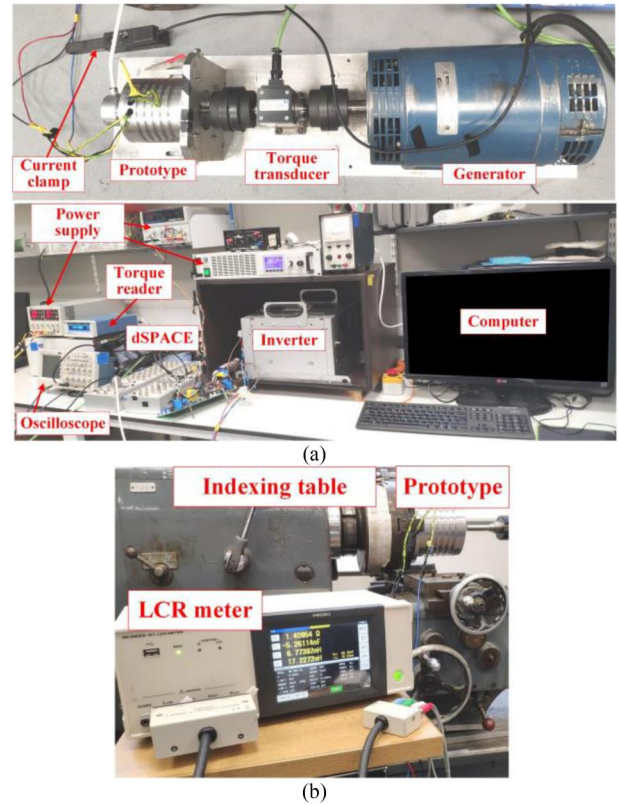


FIGURE 50 Experimental platform. (a) Dynamic, (b) Static.

400 rpm, whereas Figure 52 presents the dominant harmonics of measured back EMF. It can be observed that 12s8p CPPM machines have even order harmonics while 12s10p CPPM machines only have odd order harmonics, which validates the theoretical and FEM analyses.

7.2 | Inductances

Figures 53 and 54 compare the measured and FEM predicted phase inductance waveforms and spectra. It can be seen that the periods of the experimental results agree well with the predicted ones. The small odd order harmonics in 12s10p machines are caused by the asymmetric coil features in the winding process.

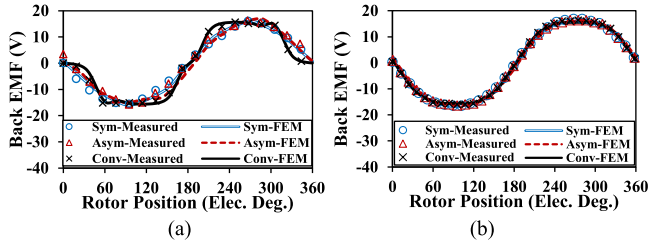


FIGURE 51 Measured and FEM predicted back EMFs at 400 rpm. (a) 12s8p machines, (b) 12s10p machines. EMF, electromotive force; FEM, finite element method.

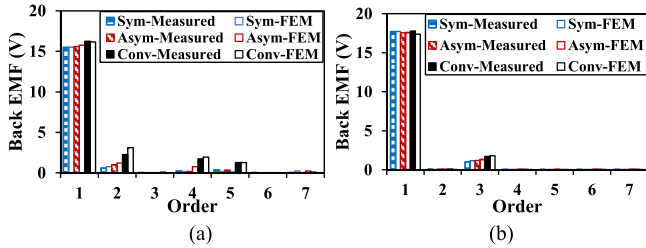


FIGURE 52 Spectrum comparisons of measured and predicted back EMFs. (a) 12s8p, (b) 12s10p. EMF, electromotive force.

7.3 | Torque waveform

By utilising the online torque transducer, the measured and predicted rated torques under $I_q = 10$ A are compared in Figures 55, 56 and Table 27. It is obvious that the 12s8p-Asym has the lowest torque ripple among all the 12s8p CPPM machines while both the 12s10p-Sym and 12s10p-Asym machines have lower torque ripple than the 12s10p-Conv machine, which confirms the FEM results. The errors are mainly caused by assembly deficiencies in the manufacturer.

In general, good agreements can be obtained in back EMFs, inductances, and torque waveforms. There are slight differences between the measured and predicted values, since the 2-dimensional FEM models are used and also the perfect manufacture and assembly of the prototype machines, are assumed.

8 | CONCLUSION

This paper has investigated the effects of slot/pole number combinations on various electromagnetic performances and effect of symmetrical and asymmetric pole shaping methods of machines with unequal north and south poles, including both CPPM and SPM machines.

For CPPM machines, when the number of coils per phase in a submachine $N_s/m/\text{GCD}(N_s, p)$ is odd, that is, the first group (e.g. 12s8p, 9s6p, 9s8p etc.), even order flux linkages and odd order inductances can be produced in windings. On the contrary, when $N_s/m/\text{GCD}(N_s, p)$ is even, that is, the second group (e.g. 12s10p, 12s14p, 6s10p etc.), the effect of unbalanced pole behaviours on windings can be eliminated, as is the

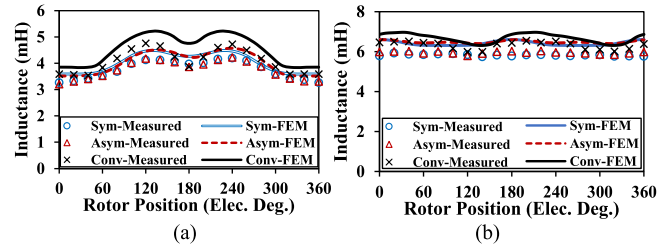


FIGURE 53 Measured and FEM predicted self-inductances. (a) 12s8p machines, (b) 12s10p machines. FEM, finite element method.

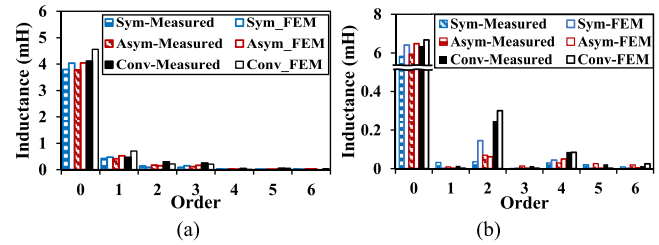


FIGURE 54 Spectrum comparisons of measured and predicted inductances. (a) 12s8p, (b) 12s10p.

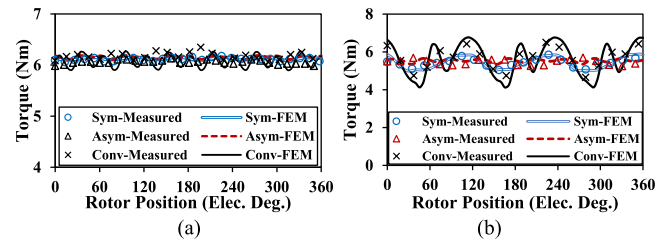


FIGURE 55 Measured and FEM predicted torque waveforms for prototypes ($I_q = 10$ A). (a) 12s8p machines, (b) 12s10p machines. FEM, finite element method.

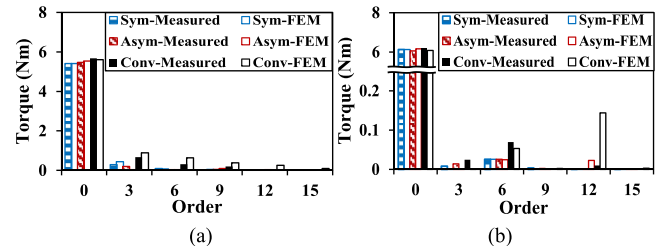


FIGURE 56 Spectrum comparisons of measured and predicted torques. (a) 12s8p, (b) 12s10p.

same case of conventional SPM machines with equal pole widths. For SPM machines, the performances, including flux linkage harmonics and torque ripples, are the same as CPPM machines, except that the harmonics of inductance for SPM machines are always 0.

For all the SPM machines and the second group CPPM machines, symmetrical pole shaping method can achieve a similar on-load torque ripple as asymmetric pole shaping method but with lower optimisation complexity. However, for the first group CPPM machines, asymmetric pole shaping method shows a better effect on torque ripple reduction, compared with symmetrical pole shaping method.

AUTHOR CONTRIBUTIONS

Ji Qi: Data curation; Formal analysis; Investigation; Methodology; Validation; Visualisation; Writing – original draft. **Ziqiang Zhu:** Conceptualisation; Funding acquisition; Investigation; Methodology; Project administration; Resources; Software; Supervision; Writing – review & editing. **Geraint Wyn Jewell:** Funding acquisition; Project administration; Supervision. **Luocheng Yan:** Investigation. **Chengwei Gan:** Project administration; Resources; Supervision. **Yuan Ren:** Project administration; Supervision. **Simon Brockway:** Funding acquisition; Project administration; Supervision. **Chris Hilton:** Funding acquisition; Project administration; Resources; Supervision.

ACKNOWLEDGEMENT

This work was supported by the UK EPSRC Future Electrical Machines Manufacturing Hub (EP/S018034/1) and Protean Electric Ltd.

CONFLICT OF INTEREST

The authors declare no conflicts of interest.

DATA AVAILABILITY STATEMENT

The data that support the findings of this study are available from the corresponding author upon reasonable request.

ORCID

Ziqiang Zhu  <https://orcid.org/0000-0001-7175-3307>
 Geraint Wyn Jewell  <https://orcid.org/0000-0002-8763-4190>

REFERENCES

1. Bailey, G., Mancheri, N., Van Acker, K.: Sustainability of permanent rare earth magnet motors in (H) EV industry. *J. Sustain. Metall.* 3(3), 611–626 (2017). <https://doi.org/10.1007/s40831-017-0118-4>
2. Hendershot, J.R., Miller, T.J.E.: *Design of Brushless Permanent Magnet Motors*. Oxford University Press, New York (1994)
3. Zhou, R., et al.: Comparative studies of fractional/integer-slot consequent pole permanent magnet machines. In: 2019 IEEE International Electric Machine and Drives Conference (IEMDC), pp. 104–111. IEEE San Diego (2019)
4. Rare Earth Permanent Magnet Machines, by Kollmorgen Technologies Corp. GB1598257A (1978)
5. Consequent Pole Permanent Magnet Rotor, by McCarty, F.B. US4631435A (1986)
6. Ghaffari, A., et al.: 2-D analytical model for outer-rotor consequent-pole brushless PM machines. *IEEE Trans. Energy Convers.* 34(4), 2226–2234 (2019). <https://doi.org/10.1109/tec.2019.2941935>
7. Chung, S.U., et al.: Fractional slot concentrated winding PMSM with consequent pole rotor for a low-speed direct drive: reduction of rare

- earth permanent magnet. *IEEE Trans. Energy Convers.* 30(1), 103–109 (2014). <https://doi.org/10.1109/tec.2014.2352365>
8. Asama, J., et al.: Development of a compact centrifugal pump with a two-axis actively positioned consequent-pole bearingless motor. *IEEE Trans. Ind. Appl.* 50(1), 288–295 (2013). <https://doi.org/10.1109/tia.2013.2270452>
9. Asama, J., et al.: Suspension performance of a two-axis actively regulated consequent-pole bearingless motor. *IEEE Trans. Energy Convers.* 28(4), 894–901 (2013). <https://doi.org/10.1109/tec.2013.2283724>
10. Xu, X., et al.: Pole optimization and thrust ripple suppression of new Halbach consequent-pole PMLSM for ropeless elevator propulsion. *IEEE Access* 8, 62042–62052 (2020). <https://doi.org/10.1109/access.2020.2984281>
11. Hu, Y., et al.: Topology optimization of a consequent-pole rotor with V-shaped magnet placement. In: 2018 21st International Conference on Electrical Machines and Systems (ICEMS), pp. 234–239. IEEE, Jeju (2018)
12. Qi, J., et al.: Effect of pole shaping on torque characteristics of consequent pole PM machines. *IEEE Trans. Ind. Appl.* 58(3), 3511–3521 (2022). <https://doi.org/10.1109/tia.2022.3156904>
13. Qi, J., et al.: Suppression of torque ripple for consequent pole PM machine by asymmetric pole shaping method. *IEEE Trans. Ind. Appl.* 58(3), 3545–3557 (2022). <https://doi.org/10.1109/tia.2022.3159629>
14. Shastri, S., Sharma, U., Singh, B.: Design of fractional-slot concentrated winding consequent pole motor for ceiling fans. In: 5th International Conference on Computing Communication and Automation (ICCCA), pp. 390–395. IEEE, India (2020)
15. Ge, X., et al.: A spoke-type IPM machine with novel alternate airspace barriers and reduction of unipolar leakage flux by step-staggered rotor. *IEEE Trans. Ind. Appl.* 52(6), 4789–4797 (2016). <https://doi.org/10.1109/tia.2016.2600649>
16. Zhu, S., et al.: Vibration reduction design of consequent pole PM machine by symmetrizing local and global magnetic field. *IEEE Trans. Ind. Electron.* 70(1), 243–254 (2023). <https://doi.org/10.1109/tie.2022.3146537>
17. Li, F., et al.: Suppression of even-order harmonics and torque ripple in outer rotor consequent-pole PM machine by multilayer winding. *IEEE Trans. Magn.* 54(11), 1–5 (2018). <https://doi.org/10.1109/tmag.2018.2839740>
18. Li, J., Wang, K., Li, F.: Reduction of torque ripple in consequent-pole permanent magnet machines using staggered rotor. *IEEE Trans. Energy Convers.* 34(2), 643–651 (2018). <https://doi.org/10.1109/tec.2018.2873318>
19. Chung, S.U., et al.: Development of a 20-pole–24-slot SPMSM with consequent pole rotor for in-wheel direct drive. *IEEE Trans. Ind. Electron.* 63(1), 302–309 (2015). <https://doi.org/10.1109/tie.2015.2472375>
20. Dhulipati, H., et al.: Torque performance enhancement in consequent pole PMSM based on magnet pole shape optimization for direct-drive EV. *IEEE Trans. Magn.* 57(2), 1–7 (2020). <https://doi.org/10.1109/tmag.2020.3026581>
21. Watahiki, T., Toriumi, Y., Miki, I.: A consequent pole motor with novel pole structure. In: 2018 International Symposium on Power Electronics, Electrical Drives, Automation and Motion (SPEEDAM), pp. 1136–1140. IEEE, Amalfi (2018)
22. Evans, S.A.: Salient pole shoe shapes of interior permanent magnet synchronous machines. In: The XIX International Conference on Electrical Machines (ICEM), pp. 1–6. IEEE, Rome (2010)
23. Li, J., et al.: Elimination of even-order harmonics and unipolar leakage flux in consequent-pole PM machines by employing NS-iron–SN-iron rotor. *IEEE Trans. Ind. Electron.* 66(3), 1736–1747 (2018). <https://doi.org/10.1109/tie.2018.2835417>
24. Bianchi, N., Bolognani, S.: Design techniques for reducing the cogging torque in surface-mounted PM motors. *IEEE Trans. Ind. Appl.* 38(5), 1259–1265 (2002). <https://doi.org/10.1109/tia.2002.802989>
25. Wang, X., et al.: Optimization of the different pole arc combination to reduce the cogging torque in PMDC motors. In: 2006 12th Biennial IEEE Conference on Electromagnetic Field Computation, pp. 367–367. IEEE (2006)

26. Zhang, H., et al.: Design considerations of novel modular-spoke-type permanent magnet machines. *IEEE Trans. Ind. Appl.* 54(5), 4236–4245 (2018). <https://doi.org/10.1109/tia.2018.2837031>
27. Ma, H., et al.: Inductance characteristic analysis of consequent-pole permanent magnet in-wheel motor. *IEEE Access* 7, 90507–90516 (2019). <https://doi.org/10.1109/access.2019.2922274>
28. Liu, Y., Zhu, Z.Q., Howe, D.: Direct torque control of brushless DC drives with reduced torque ripple. *IEEE Trans. Ind. Appl.* 41(2), 599–608 (2005). <https://doi.org/10.1109/tia.2005.844853>
29. Yan, L., et al.: Torque ripple suppression of permanent magnet synchronous machines by minimal harmonic current injection. *IET Power Electron.* 12(6), 1368–1375 (2019). <https://doi.org/10.1049/iet-pel.2018.5647>
30. Zhu, Z.Q., Howe, D.: Influence of design parameters on cogging torque in permanent magnet machines. *IEEE Trans. Energy Convers.* 15(4), 407–412 (2000). <https://doi.org/10.1109/60.900501>
31. Zhu, L., et al.: Analytical methods for minimizing cogging torque in permanent-magnet machines. *IEEE Trans. Magn.* 45(4), 2023–2031 (2009). <https://doi.org/10.1109/tmag.2008.2011363>
32. Zhu, Z.Q., Chu, W.Q.: Advanced frozen permeability technique and applications in developing high performance electrical machines. *Trans. China Electrotech. Soc.* 31(20), 13–29 (2016)
33. Du, Z.S., Lipo, T.A.: High torque density and low torque ripple shaped-magnet machines using sinusoidal plus third harmonic shaped magnets. *IEEE Trans. Ind. Appl.* 55(3), 2601–2610 (2019). <https://doi.org/10.1109/tia.2019.2896014>

How to cite this article: Qi, J., et al.: Influence of slot/pole number combinations and pole shaping on electromagnetic performance of permanent magnet machines with unbalanced north and south poles. *IET Electr. Power Appl.* 1–28 (2023). <https://doi.org/10.1049/elp2.12293>